

Geometry and purity properties of qudit Hamiltonian systems

J.A. López–Saldívar^{1,2,3}, O. Castaños^{4,†}, S. Cordero⁴, E. Nahmad–Achar⁴ and R. López–Peña⁴

¹ Department of Theoretical Physics, Moscow Institute of Physics and Technology, Dolgoprudnyi 141700, Russia

² Russian Quantum Center, Skolkovo, Moscow 143025, Russia

³ National University of Science and Technology “MISIS”, Moscow 119049, Russia

⁴ Instituto de Ciencias Nucleares, Universidad Nacional Autónoma de México, Apartado Postal 70-543, 04510 Mexico City, Mexico

[†] On sabbatical leave at University of Granada, Spain

E-mail: julio.lopez.8303@gmail.com, ocasta@nucleares.unam.mx,
sergio.cordero@nucleares.unam.mx, nahmad@nucleares.unam.mx, lopez@nucleares.unam.mx

Abstract

The principle of maximum entropy is used to study the geometric properties of an ensemble of finite dimensional Hamiltonian systems with known average energy. These geometric characterization is given in terms of the generalized diagonal Bloch vectors and the invariants of the special unitary group in n dimensions. As examples, Hamiltonians written in terms of linear and quadratic generators of the angular momentum algebra are considered with $J = 1$ and $J = 3/2$. For these cases, paths as functions of the temperature are established in the corresponding simplex representations, as well as the adiabatic evolution of the interaction strengths of the Hamiltonian models. For the Lipkin-Meshkov-Glick Hamiltonian the quantum phase diagram is explicitly shown for different temperature values in parameter space.

Keywords: *purity, thermal qudit states, geometric properties, maximum entropy, invariant spaces, LMG model*

1. Introduction

Quantum information theory has become an important tool in the study of physical systems. Although the processing of quantum information is still a young field of research, it has yielded a deep change about the fundamental aspects of quantum mechanics. The main purpose of this field is the exploitation of the quantum features with a technological purpose [1–4]. Differences between classical and quantum information are related to the possibility of having secure communications, to the solution of certain mathematical problems, and perhaps to having a quantum computer. All these benefits are due to properties of quantum mechanics such as uncertainty, interference, and entanglement. Thus, it becomes important to study the entanglement properties of quantum states, which implies the characterization of the entanglement, its application to quantum information processing and, from the mathematical point of view, the characterization and classification of positive maps on C^* algebras [2–4].

The first explicit relation made between physical entropy and information is associated to the relation between energy and information. This goes back to Maxwell’s demon paradox introduced in 1867, which implies an apparent violation of the second law of thermodynamics. The connection of information theory to physics helps to solve Maxwell’s demon paradox with the establishment of Landauer’s principle, that is, energy can be extracted from information [5,6]. Shannon [7] establishes that if a message has n symbols having transmission probabilities (p_1, p_2, \dots, p_n) the amount of information in the message is,

$$\mathcal{H}_S = - \sum_{i=1}^n p_i \ln p_i. \quad (1)$$

He called this quantity *uncertainty*, but von Neumann asked him to call it entropy arguing that a similar expression exists in statistical mechanics [6].

E. Jaynes in 1957 established that Shannon had actually uncovered a fundamental element of probability theory, that is, $\mathcal{H}_S \equiv S$ defines the entropy of a probability distribution on an exhaustive set of mutually exclusive alternatives. The principle of maximum entropy PME establishes that *the distribution $\{p_k\}$ that maximizes S subject to the constraints imposed by the available information is the least biased description of what we know about the set of alternatives* [8–10]. It has been proven that the PME is a correct method of inference when new information is given in terms of expectation values [11].

This rule provides a variational procedure for constructing prior probabilities on a given evidence. If we do not know something about a system, this rule establishes that the system has the same probability of staying in any of all its possible states, i.e., $p_\ell = 1/n$ and $S = \ln n$. If the system is in one particular state k , one has $S = 0$. If the expectation value of the energy is known, the PME determines the Gibbs canonical ensemble, if the energy and number of moles are known one gets the Gibbs grand canonical ensemble, if the expectation values of the energy and angular momentum are known the PME determines the Gibbs rotational ensemble [12]. Additionally, the use of the PME for physical systems in thermal equilibrium can be extended to solve non-equilibrium problems because it can be applied to any physical quantity, be it density of particles, density of kinetic energy, components of the stress tensor, intensity of the magnetization, and so on.

Collective spin operators of multi-qudit systems generate a unitary algebra in n dimensions, $u(n)$, and the concepts of pairwise entanglement and spin squeezing has been extended to describe general multi-qudit systems. The reduced density matrices of one and two qudits in the system of symmetric multi-qudits are used to determine, by means of the linear and von Neumann entropies, their entanglement properties. For the squeezing concept an embedding of the $su(2)$ sub-algebras into $u(n)$ is proposed, which yields n squeezing parameters. Both the entanglement and the squeezing parameters are good markers of the quantum phase transitions exhibited by the Lipkin-Meshkov-Glick Hamiltonian system of n level interacting atoms and thus they can be used to establish the corresponding quantum information diagrams, and also through the inverse participation ratio concept to determine the corresponding localization properties in phase space [13–15].

There are several basis states for finite n -dimensional systems: The generalized Gell-Mann vectors, those associated to the generators of the special unitary algebras $SU(n)$, the polarization operators, the Weyl operators, the Casimir invariants of $SU(n)$, and the canonical coset decomposition of unitary matrices [16–20]. In particular, we will consider in this work the generalized Bloch vectors because they allow us to determine the density matrix on the basis of actual measurements. The density matrix description of a state of n -level systems requires $n^2 - 1$ real parameters and it can be written in the form [18, 20, 21]

$$\boldsymbol{\rho} = \frac{1}{n} \mathbf{I} + \frac{1}{2} \sum_{k=1}^{n^2-1} \lambda_k \boldsymbol{\Lambda}_k, \quad (2)$$

where \mathbf{I} is the identity matrix in n dimensions and λ_k is the expectation value of the generator $\boldsymbol{\Lambda}_k$. The operator $\boldsymbol{\rho}$ is hermitian and satisfies $\text{Tr}(\boldsymbol{\rho}) = 1$ because the generators $\boldsymbol{\Lambda}_k$ of the special unitary algebra $SU(n)$ are complex traceless hermitian matrices. These generators have the property $\text{Tr}(\boldsymbol{\Lambda}_j \boldsymbol{\Lambda}_k) = 2 \delta_{jk}$.

The important properties for the description of the density matrix state are the positivity condition $\boldsymbol{\rho}_k \geq 0$ and the fact that $1/n \leq \text{Tr}(\boldsymbol{\rho}^2) \leq 1$, which are fundamental to determine the physical space of the density matrices [22, 23]. Notice that the generators are determined by means of the symmetric d_{ijk} and antisymmetric f_{ijk} structure constants of the mentioned special unitary algebra. The condition, $\text{Tr}(\boldsymbol{\rho}^2) \leq 1$ on (2) implies that the length of the Bloch vector is bounded, that is,

$$|\lambda| \leq \sqrt{\frac{2(n-1)}{n}}. \quad (3)$$

The density matrix (2) satisfies the positivity condition if its characteristic polynomial $p_\rho(x) = \det(x\mathbf{I} - \boldsymbol{\rho})$, viz.

$$p_\rho(x) = x^n - a_1 x^{n-1} + a_2 x^{n-2} - \dots + (-1)^{n-1} a_{n-1} x + (-1)^n a_n, \quad (4)$$

has coefficients $a_k \geq 0$ according to the Descartes theorem about the sign rules [24].

An additional remark is that the orbits generated by unitary transformations on the density matrices can be classified in terms of the Gram matrix, built from the Hilbert-Schmidt scalar products of the vectors lying in the tangent space of the orbits, and the rank of the Gram matrix determines the dimensions of the orbits. This classification is consistent with the results obtained by means of the stability groups of unitary transformations [25, 26]. Due to the invariance of the Gram matrix under unitary transformations, in order to determine the orbits one can consider the diagonal representation of the density matrix [27–30].

An interesting feature of unitary group representations for quantum systems is their correspondence with different projective geometries as the Fano projective plane [31] with the 2-simplex of the qutrit system, or the projective space $\text{PG}(3,2)$ [32] with the 3-simplex defined for a four-level system. See [33] and references therein for a study and historical perspective of the connection between quantum information processes to projective geometries and combinatorial design.

In this contribution, the physical space associated to the diagonal generalized Bloch vectors and the Casimir invariants is determined, in order to describe the well-defined density matrices of systems of qubits, qutrits, and ququarts. We use the PME to determine the density matrices of ensembles of qubits, qutrits, and ququarts with a defined average energy. These ensembles are described by Hamiltonians given in terms of linear and quadratic generators of the angular momentum algebra. By means of the diagonal decomposition of the density matrices associated to the linear and quadratic Hamiltonians, we may visualize geometrically the purity properties of ensembles with known average energy. In particular, the available paths in the corresponding simplex representations are established for the ensembles as a function of the temperature.

Section 2 gives a description of the Principle of Maximum Entropy for an ensemble of particles with a fixed averaged energy, which yields the Boltzmann probability density and at the same time minimizes the Helmholtz free energy of the quantum system. Different matrix representations of a density operator of an n dimensional quantum system are also given, these being the probability, the Bloch-Gell-Mann, and the invariant cases. In addition, a general discussion of the thermal trajectories as a function of the temperature are given, from $T \rightarrow 0$ (pure state) to $T \rightarrow \infty$ (the most mixed state). In section 3 the diagonal representations for the qutrit and ququart systems are established together with the corresponding mapping between them. Thus, one is able to exhibit the localization of the physical density matrices in the probability (p)-, Gell-Mann (λ)-, and invariant (t)-spaces, with and without eigenvalue degeneracy, the latter of which is associated to the higher dimensional orbits of the qutrit and ququart systems. In section 4, linear and quadratic Hamiltonian models in terms of the angular momentum operators are considered, particularly for $J = 1$ (a realization in terms of identical but distinguishable dimers) and $J = 3/2$ (a realization in terms of identical but distinguishable trimers). The behavior of the thermal states for the qutrit and ququart is obtained and visualized in the p -, λ - and t -spaces. For the Lipkin-Meshkov-Glick Hamiltonian model particular attention is paid to the quantum phase transitions and their influence on the characteristics of the corresponding thermal states in the diagonal representation. Section 5 gives a summary of the main results and additional remarks.

2. Variational thermal density matrix.

In quantum statistical mechanics the entropy is defined in terms of the density matrix

$$S = -k_B \text{Tr}(\rho \ln \rho), \quad (5)$$

with the constraints $\text{Tr} \rho = 1$ and $\text{Tr} \rho^2 \leq 1$. If one considers n finite dimensional systems, the density

operator has also another restriction $\text{Tr} \boldsymbol{\rho}^2 \geq 1/n$. According to the PME, the *prior* knowledge of an ensemble of quantum systems can be used to maximize the entropy. If the average energy $\text{Tr}(\boldsymbol{\rho} \mathbf{H}) = \bar{E}$ is known, one must then take the following variations: $\delta S = 0$, $\delta(\text{Tr} \boldsymbol{\rho} - 1) = 0$, and $\delta(\text{Tr}(\boldsymbol{\rho} \mathbf{H}) - \bar{E}) = 0$, implying that [34]

$$\text{Tr} [(1 + \ln \boldsymbol{\rho} + \epsilon + \beta \mathbf{H}) \delta \boldsymbol{\rho}] = 0, \quad (6)$$

where we have introduced two Lagrange multipliers ϵ and β . From the last expression one obtains the density matrix $\boldsymbol{\rho}$ and, taking its trace, ϵ is determined, yielding

$$\boldsymbol{\rho} = \frac{1}{Z} \exp(-\beta \mathbf{H}), \quad (7)$$

with the partition function $Z = \text{Tr} [\exp(-\beta \mathbf{H})]$. In order to determine β , one considers a cavity filled with photons in thermal equilibrium with the walls at temperature T . In this case, and by means of the *Correspondence Principle*, one obtains $\beta = \frac{1}{k_B T}$. Notice that the maximization requirement of the entropy yields the expression

$$TS - U + F = 0, \quad (8)$$

with the identification of the internal energy of the system $U = \langle \mathbf{H} \rangle$ and the Helmholtz free energy $F = -k_B T \ln Z$. Therefore the PME implies also a minimum Helmholtz free energy of the system.

Expression (7) may be obtained by considering a closed system constituted by the Hamiltonian associated to one subsystem and the Hamiltonian of a heat bath, in which the interaction term can be ignored. In this case the composed system can also be represented by a micro-canonical ensemble in the energy interval E and $E + \delta E$ with $\delta E \ll E$. If the number of degrees of freedom of the bath is very large the reduced density matrix takes the form given in Eq. (2). This procedure has led to the answer of when is it possible to represent the reduced density matrix of the system $\boldsymbol{\rho}_S$ in terms of a wave function ψ with $\boldsymbol{\rho}_\psi = \boldsymbol{\rho}_S$ [35–37].

Note, once again, that the variational method maximizes the von Neumann entropy and simultaneously minimizes the energy.

2.1. Matrix representations.

In order to study finite mixed quantum systems the use of the density matrix formalism is necessary. Besides (*vide infra*), to consider its diagonal form is convenient if one wishes to classify the different types of density matrices according to the dimension of the orbits in the tangent space.

The set of diagonal density matrices of dimension n can be denoted in terms of their eigenvalues,

$$\mathbf{D}_n = \text{DiagM} (p_1, p_2, \dots, p_{n-1}, p_n), \quad (9)$$

with $0 \leq p_k \leq 1$ and $\sum_{k=1}^n p_k = 1$. This set then forms a simplex in $n - 1$ dimensions (cf. e.g. [38]). A general density matrix can be constructed from them via

$$\boldsymbol{\rho} = \mathbf{U} \mathbf{D}_n \mathbf{U}^\dagger, \quad (10)$$

where \mathbf{U} denotes a unitary transformation in n dimensions, $\text{U}(n)$. The set of transformations leaving \mathbf{D}_n invariant form a group called the stability group \mathcal{H} , i.e.,

$$\mathbf{T}_{\mathcal{H}} \mathbf{D}_n \mathbf{T}_{\mathcal{H}}^\dagger = \mathbf{D}_n \quad \rightarrow \quad \boldsymbol{\rho} = \boldsymbol{\Omega} \mathbf{D}_n \boldsymbol{\Omega}^\dagger, \quad (11)$$

with $\boldsymbol{\Omega}$ being an element of the quotient group $\text{U}(n)/\mathcal{H}$ and the unitary transformation can be decomposed as $\mathbf{U} = \boldsymbol{\Omega} \mathbf{T}_{\mathcal{H}}$. This result allows us to characterize the $n \times n$ density matrices by the

orbit of a point in \mathbf{D}_n under the action of the quotient group $U(n)/\mathcal{H}$. This can be done by denoting the degeneracy of the eigenvalues p_j by

$$\mathcal{M} = \{m_1, m_2, \dots, m_{\ell-1}, m_\ell\}, \quad (12)$$

with $\sum_{k=1}^{\ell} m_k = 1$. Then the stability group is defined by the tensorial product

$$\mathcal{H} = U(m_1) \otimes U(m_2) \otimes \dots \otimes U(m_\ell). \quad (13)$$

The quotient group is called a complex flag manifold denoted by

$$\mathcal{F} = U(n)/(U(m_1) \otimes \dots \otimes U(m_\ell)). \quad (14)$$

These mathematical results [39] are going to be applied for the particular Hamiltonian systems considered here, viz., the linear and quadratic Hamiltonians in terms of the angular momentum generators.

The generators of an n dimensional unitary group can be characterized by the operators $\mathbf{A}_{kj} = |k\rangle\langle j|$ with $j, k = 1, 2, \dots, n$, and through them any unitary matrix can be constructed,

$$(\boldsymbol{\rho})_{jk} := \langle j|\boldsymbol{\rho}|k\rangle = \text{Tr}[\boldsymbol{\rho}\mathbf{A}_{kj}] \quad (15)$$

where $\mathbf{A}_{kj}\mathbf{A}_{\ell m} = \delta_{j\ell}\mathbf{A}_{km}$. The positive coefficient $p_j := (\boldsymbol{\rho})_{jj}$ denotes the probability to find the system in the state given by the projector $\mathbf{P}_j := \mathbf{A}_{jj}$, while the non-diagonal elements $a_{jk} := (\boldsymbol{\rho})_{jk}$ stand for the probability amplitude for the transition $|k\rangle \rightarrow |j\rangle$. Then, in general, a density matrix can be written as,

$$\boldsymbol{\rho} = \sum_{j=1}^n p_j \mathbf{P}_j + \sum_{j \neq k} a_{jk} \mathbf{A}_{jk}; \quad a_{kj} = a_{jk}^* \wedge \text{Tr}[\boldsymbol{\rho}] = 1, \quad (16)$$

together with the positivity condition. One should note that, if the non-diagonal terms fulfil $a_{jk} = \sqrt{p_j p_k} e^{i(\theta_k - \theta_j)}$ then $\boldsymbol{\rho}$ represents a pure state $\text{Tr}(\boldsymbol{\rho}^2) = 1$.

A special unitary algebra in n dimensions can be denoted by a set of operators $\mathbf{\Lambda}_k$ with $k = 1, 2, \dots, n^2 - 1$. They are traceless $\text{Tr}(\mathbf{\Lambda}_k) = 0$ and satisfy that $\text{Tr}(\mathbf{\Lambda}_j \mathbf{\Lambda}_k) = 2\delta_{jk}$. Further, these operators can be generated by the symmetric and antisymmetric linear combinations [18, 40],

$$\mathbf{A}_{jk} + \mathbf{A}_{kj}, \quad -i(\mathbf{A}_{jk} - \mathbf{A}_{kj}), \quad j < k. \quad (17)$$

together with the diagonal matrices defined by

$$(\mathbf{F}_\ell)_{rr} = \sqrt{\frac{2}{\ell(\ell+1)}} \begin{cases} 1 & r \leq \ell, \\ -\ell & r = \ell + 1, \\ 0 & r > \ell + 1, \end{cases} \quad (18)$$

with $\ell = 1, 2, \dots, n-1$. Typically they are ordered, describing first the symmetric $n(n-1)/2$, then the antisymmetric $n(n-1)/2$, and at the end the diagonal matrices $(n-1)$. In this order, the diagonal Gell-Mann matrices are labeled as

$$\mathbf{\Lambda}_{k_\ell} := \mathbf{F}_\ell; \quad k_\ell := n^2 - n + \ell, \quad \ell = 1, 2, \dots, n-1. \quad (19)$$

- (i) *Probability representation.* The simplest representation is to consider the set of probability values for a fixed set of projectors \mathbf{P}_j , i.e., $p_j = \text{Tr}[\boldsymbol{\rho}\mathbf{P}_j]$, which defines a probability-space referred to as the p -space. In particular, if the density matrix $\boldsymbol{\rho}$ is given in terms of its eigen-projectors, i.e., when $\boldsymbol{\rho}\mathbf{P}_j = p_j\mathbf{P}_j$ is fulfilled for each \mathbf{P}_j , the matrix is written in a diagonal form as

$$\boldsymbol{\rho} = \sum_{j=1}^n p_j \mathbf{P}_j := \text{DiagM}(p_1, p_2, \dots, p_n); \quad \mathbf{P}_j \mathbf{P}_k = \delta_{jk} \mathbf{P}_j. \quad (20)$$

This set of projectors defines a subset of density matrices which commute with each other $[\boldsymbol{\rho}, \boldsymbol{\rho}'] = 0$. By using the constrictions

$$\sum_{j=1}^n p_j = 1; \quad 0 \leq p_j \leq 1 \quad \forall j,$$

one obtains the set of points $\vec{p} = (p_1, p_2, \dots, p_n)$ defining a section of a hyperplane in the n -dimensional space, for which each point of the simplex in the p -space represents a physical state of the system, and each vertex \vec{p}_j (with $p_j = 1$) a pure state. Note that the relation of one point in the simplex with one physical state is unique only when the diagonal matrix $\boldsymbol{\rho}$ is written in the fixed set of its eigen-projectors \mathbf{P}_j , because the p -space forgets the physical nature of the problem.

(ii) *Gell-Mann representation.* Using the Gell-Mann operators $\mathbf{\Lambda}_j$ one may write any density matrix as

$$\boldsymbol{\rho} = \frac{1}{n} \mathbf{I} + \frac{1}{2} \sum_{j=1}^{n^2-1} \lambda_j \mathbf{\Lambda}_j; \quad \text{Tr}[\mathbf{\Lambda}_j] = 0; \quad \text{Tr}[\mathbf{\Lambda}_j \mathbf{\Lambda}_k] = 2\delta_{jk}. \quad (21)$$

Since $\mathbf{\Lambda}_j$ are traceless operators, a direct comparison between equations (21) and equations (16) for the diagonal representation of a density matrix, shows that one may choose $n-1$ diagonal operators, providing the $n-1$ free parameters $\vec{\lambda} = (\lambda_{k_1}, \lambda_{k_2}, \dots, \lambda_{k_{n-1}})$ defining an $(n-1)$ -dimensional space (referred to as the λ -space hereafter). By using the diagonal operators (19), one establishes the relationship between the free λ_{k_j} ($k_j = n^2 - n + j$) parameters and probabilities $p_s = \text{Tr}[\boldsymbol{\rho} \mathbf{A}_{ss}]$ as

$$p_s = \frac{1}{n} + \frac{1}{2} \sum_{\ell=1}^{n-1} a_{k_\ell s} \lambda_{k_\ell}, \quad a_{k_\ell s} := (\mathbf{\Lambda}_{k_\ell})_{ss}, \quad s = 1, 2, \dots, n.$$

The set of values $a_{\ell s}$ and the constriction $0 \leq p_s \leq 1$ yield the set of acceptable values $\vec{\lambda}$ in the λ -space for which the matrix $\boldsymbol{\rho}$ represents a physical state of the system. Notice that the relationship between probabilities and the free parameters $\vec{\lambda}$ is linear, so each point in p -space is mapped to one and only one point in λ -space, and hence the transformation is invertible, i.e., the map

$$\vec{p} = \mathbf{M} \vec{\Lambda}; \quad \vec{\Lambda} := (\lambda_{k_1}, \lambda_{k_2}, \dots, \lambda_{k_{n-1}}, 1), \quad (22)$$

with

$$\mathbf{M} = \frac{1}{2} \begin{pmatrix} a_{k_1 1} & a_{k_2 1} & \dots & a_{k_{n-1} 1} & 2/n \\ a_{k_1 2} & a_{k_2 2} & \dots & a_{k_{n-1} 2} & 2/n \\ \vdots & \vdots & \ddots & \vdots & \vdots \\ a_{k_1 n} & a_{k_2 n} & \dots & a_{k_{n-1} n} & 2/n \end{pmatrix},$$

has inverse matrix \mathbf{M}^{-1} . Clearly, the zero vector $\vec{\lambda}_e$ or $\vec{\Lambda}_e = (0, 0, \dots, 0, 1)$ represents the most entangled state; while the set of pure states are given by the set of vectors $\vec{\Lambda}_j$ for which $\vec{p}_j = \mathbf{M} \vec{\Lambda}_j$, and each one of these corresponds to a vertex in the λ -space.

(iii) *Invariants representation.* An alternative form to characterize a set of density matrices of dimension n is via the named invariants $t_s := \text{Tr}[\boldsymbol{\rho}^s]$ for $s = 1, 2, \dots$. Besides $t_1 = 1$, it is a fact that there are $n-1$ invariants which are independent; typically, the first ones are considered, i.e.,

$$t_\ell := \text{Tr}[\boldsymbol{\rho}^\ell]; \quad \ell = 1, 2, \dots, n. \quad (23)$$

This means that any invariant t_s for $s > n$ can be given in terms of t_1, t_2, \dots, t_n . Since $t_1 = 1$ is a constant, the set of invariants defines an $(n-1)$ -dimensional space, the *invariants-space*, hereafter referred to as t -space, with points of the form $\vec{t} = (t_2, t_3, \dots, t_n)$, each delimited by the condition

$$\frac{1}{n^{\ell-1}} \leq t_\ell \leq 1 \quad \ell = 2, 3, \dots, n,$$

where the lower and upper bounds are calculated for the most entangled and the pure states, respectively. Similar to the simplex in the p -space or λ -space, the region of the t -space for which each point defines a physical state of the system has n vertices, given by

$$\vec{t}_k := \left(\frac{1}{k}, \frac{1}{k^2}, \dots, \frac{1}{k^{n-1}} \right); \quad k = 1, 2, \dots, n. \quad (24)$$

The points \vec{t}_1 and \vec{t}_n correspond to the pure and most entangled state, respectively. The other ones, \vec{t}_k with $k \neq 1$ and $k \neq n$, correspond to the k -maximum entangled states, i.e., states composed with only k pure states. Thus, for a fixed set of pure states, each vertex represents

$$N_k = \frac{n!}{k!(n-k)!},$$

physical states, while any other point $\vec{t} \neq \vec{t}_k$ represents $n!$ physical states; in other words one may map the simplex to the t -space, but this map is not invertible.

Therefore one can study and visualize the behavior of any finite dimensional density matrix in each of the matrix representations considered in the section, that is, in the p -, λ -, and t - spaces. Examples of interest can be the following: (i) the temporal unitary evolution of a mixed state constituted by a linear combination of energy eigenstates, multiplied by coefficients p_k satisfying that $p_k \geq 0$ and $\sum_k p_k = 1$; (ii) the adiabatic evolution of the parameters appearing in a Hamiltonian operator and yielding quantum phase transitions; and (iii) the movement in the mentioned spaces when the temperature between the system and the bath is changing. (iv) Finally, the use of a master equation to determine a non-unitary temporal evolution of a quantum system may also be studied.

2.2. Thermal density matrix at endpoints.

In this work, we are interested in studying the case for Hamiltonians with a finite number of accesibles energy levels; in this case one has two limit points, viz. $\beta \rightarrow 0$ (infinite temperature) and $\beta \rightarrow \infty$ (zero temperature). Without loss of generality, one may consider the case of n -level systems and that the energy spectrum has been sorted in an increasing form, i.e.,

$$h_1 \leq h_2 \leq \dots \leq h_n.$$

The thermal matrix density matrix Eq. (7) in the Hamiltonian basis is a diagonal matrix, i.e.,

$$\rho_D = \text{DiagM} (p_1, p_2, \dots, p_n); \quad p_j = \frac{e^{-\beta h_j}}{\sum_{k=1}^n e^{-\beta h_k}},$$

and in the limits one has:

- (i) Case $\beta \rightarrow 0$, in this case all values p_j go to a constant

$$\lim_{\beta \rightarrow 0} p_j \rightarrow \frac{1}{n},$$

representing the most entangled state, where any eigenstate of the system is accesible with the same probability.

- (ii) Case $\beta \rightarrow \infty$, for this case one finds that any value p_j corresponding to an excited state ($h_j > h_1$) vanishes, while for states with the ground energy ($h_j = h_1$) one has

$$\lim_{\beta \rightarrow \infty} p_j \rightarrow \frac{1}{k},$$

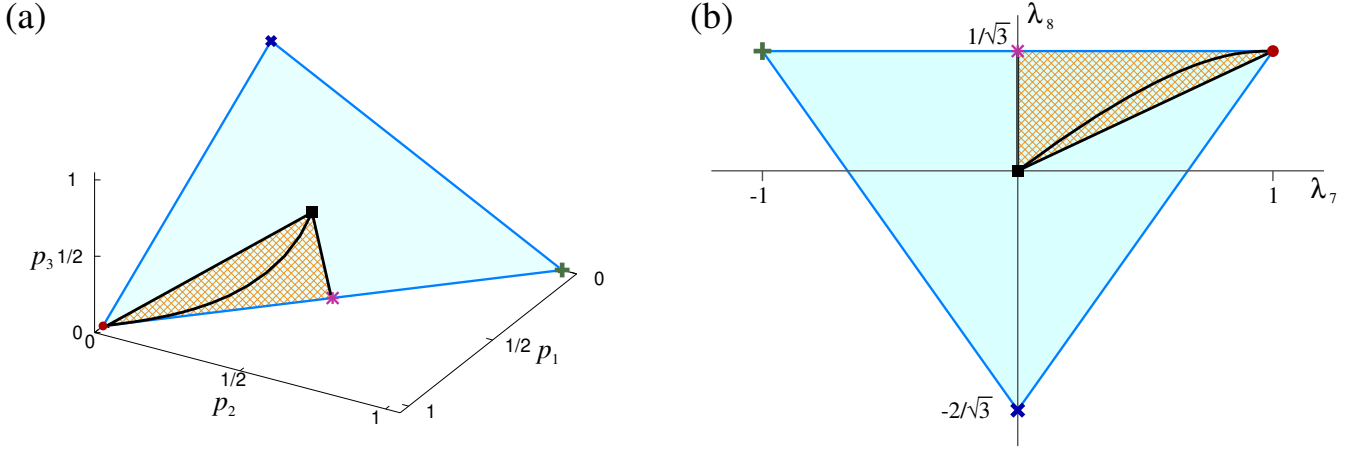


Figure 1. The simplex region in p -space (a), and the projection from the p -space to the λ -space (b), are shown for a 3-level system. In both cases, the vertices representing pure states are indicated by a dot-symbol (occupation probability of the ground state), plus-symbol (occupation probability of the first excited state) and times-symbol (occupation probability of the second excited state). The central square-symbol point represents the most mixed state, and the asterisk-symbol the middle point between p_1 and p_2 . Solid black lines correspond to the points of the thermal state as a function of the temperature, so the straight line from the vertex corresponds to starting from a pure ground state; the straight line which connects the central point with the middle point along the edge corresponds to the case of two degenerate occupation probabilities of the ground state; and the black curve shows the qualitative behavior for the general case of a density matrix without degenerate eigenvalues.

where k stands for the degeneracy of the ground state of the system. In this sense, the density matrix goes to a particular ground state projector, with equal probability for each fixed ground state in the basis, as expected because Eq. (7) is the density matrix for the ground state with maximum entropy for finite temperature.

The endpoints of the thermal state correspond to the vertices Eq. (24) of the physical t -space in the invariants representation.

These results are independent of the matrix representation of the density matrix. So, in the p -space the thermal density matrix as a function of the temperature moves from a vertex (or the middle point in the (simplex edge) subspace of degenerate ground state energy) to the simplex central point (the most mixed state) along a trajectory (cf. Fig. 1 and the discussion in Subsection 3.1). A similar result is obtained in the λ -space for the Gell-Mann representation, while in the t -space this trajectory is from the vertex \vec{t}_k (with k the degeneracy of ground state) to the vertex \vec{t}_n .

We should stress that to consider the density matrix in its diagonal representation facilitates the study of its properties as function of the set of variables involved in an n -dimensional quantum system.

3. Geometric properties of the qutrit and ququart systems.

To describe the general properties of the qutrit and ququart systems, we use their corresponding diagonal representations. A qutrit system has a geometric representation in a hyperplane of a 3-dimensional space (p -space) or in a 2-dimensional space (λ - and t -spaces), while the ququart system requires of an hyperplane in a 4-dimensional space (p -space) or a 3-dimensional space (λ - and t -space). Here, we review these representations for general diagonal density matrices, i.e., we suppose that the density matrix of

the qutrit is given by $\boldsymbol{\rho} = \text{DiagM}(\rho_{11}, \rho_{22}, \rho_{33})$ and for the ququart $\boldsymbol{\rho} = \text{DiagM}(\rho_{11}, \rho_{22}, \rho_{33}, \rho_{44})$, and point out some interesting features of their representations.

3.1. Qutrit system

In the probability representation, the numerical eigenvalues are limited by the normalization condition $\text{Tr } \boldsymbol{\rho}_D = 1$, i.e., $p_1 + p_2 + p_3 = 1$, and by the probabilistic interpretation of the eigenvalues of the density matrix $0 \leq p_j \leq 1$ ($j = 1, 2, 3$). The spanned space from these conditions is the simplex shown in Fig. 1(a) whose vertices are located at $\vec{p}_1 := (1, 0, 0)$, $\vec{p}_2 := (0, 1, 0)$, and $\vec{p}_3 := (0, 0, 1)$. These three points depict each one of the pure states ($\text{Tr } \boldsymbol{\rho}^2 = 1$) with one eigenvalue equal to one and the other two equal to zero. The edges delimiting the triangle are parametrized by

$$\vec{p}_{jk} = \vec{p}_j + (\vec{p}_k - \vec{p}_j)x; \quad x \in [0, 1]; \quad j, k = 1, 2, 3 \wedge j < k, \quad (25)$$

which correspond to all the possible quantum states with one eigenvalue equal to zero. The set of states with at least two equal probability values is parametrized by

$$\vec{p}_{jkl} = \vec{p}_j + \left(\frac{1}{2} [\vec{p}_k + \vec{p}_\ell] - \vec{p}_j \right) x; \quad x \in [0, 1]; \quad j \neq k \wedge j \neq \ell \wedge k \neq \ell, \quad (26)$$

and note that $\vec{p}_{jkl} = \vec{p}_{\ell k j}$. The centroid of the simplex is given by the point $\vec{p}_e = (1/3, 1/3, 1/3)$ representing the most mixed state of the system.

The explicit form of the diagonal density matrix operator in the λ -space is given by

$$\boldsymbol{\rho} = \text{DiagM} \left(\frac{1}{3} + \frac{\lambda_7}{2} + \frac{\lambda_8}{2\sqrt{3}}, \frac{1}{3} - \frac{\lambda_7}{2} + \frac{\lambda_8}{2\sqrt{3}}, \frac{1}{3} - \frac{\lambda_8}{\sqrt{3}} \right). \quad (27)$$

which allows us to describe the system by two variables λ_7 and λ_8 . For example, the conditions $0 \leq \rho_{jj} \leq 1$ allow us to define the area of the space in which the values of λ_7 and λ_8 define a quantum system. These conditions can be written as

$$-1 \leq \lambda_7 \leq 1, \quad \frac{-2 + 3|\lambda_7|}{\sqrt{3}} \leq \lambda_8 \leq \frac{1}{\sqrt{3}}, \quad (28)$$

which defines a triangle with vertices at $(1, 1/\sqrt{3})$, $(-1, 1/\sqrt{3})$, and $(0, -2/\sqrt{3})$, corresponding to the pure states with density matrices $\text{DiagM}(1, 0, 0)$, $\text{DiagM}(0, 1, 0)$, and $\text{DiagM}(0, 0, 1)$, respectively.

Since the simplexes in p -space and λ -space are related through a linear map, we consider first these representations, by choosing the diagonal Gell-Mann operators as

$$\boldsymbol{\Lambda}_7 = \text{DiagM}(1, -1, 0); \quad \boldsymbol{\Lambda}_8 = \frac{1}{\sqrt{3}} \text{DiagM}(1, 1, -2).$$

Notice that the Gell-Mann vector is reduced to only two components different from zero. We have the matrix transformation $\vec{p} = \boldsymbol{M} \vec{\Lambda}$ with $\vec{p} = (p_1, p_2, p_3)$, $\vec{\Lambda} = (\lambda_7, \lambda_8, 1)$ and

$$\boldsymbol{M} = \frac{1}{2} \begin{pmatrix} 1 & \frac{1}{\sqrt{3}} & \frac{2}{3} \\ -1 & \frac{1}{\sqrt{3}} & \frac{2}{3} \\ 0 & -\frac{2}{\sqrt{3}} & \frac{2}{3} \end{pmatrix}; \quad \boldsymbol{M}^{-1} = \begin{pmatrix} 1 & -1 & 0 \\ \frac{1}{\sqrt{3}} & \frac{1}{\sqrt{3}} & -\frac{2}{\sqrt{3}} \\ 1 & 1 & 1 \end{pmatrix}; \quad (29)$$

the two dimensional λ -space is given by the points $\vec{\Lambda} := (\lambda_7, \lambda_8)$, so the vertices in the p -simplex are changed to vertices in the λ -space as

$$\vec{p}_1 \rightarrow \vec{\Lambda}_1 = \left(1, \frac{1}{\sqrt{3}} \right); \quad \vec{p}_2 \rightarrow \vec{\Lambda}_2 = \left(-1, \frac{1}{\sqrt{3}} \right); \quad \vec{p}_3 \rightarrow \vec{\Lambda}_3 = \left(0, -\frac{2}{\sqrt{3}} \right);$$

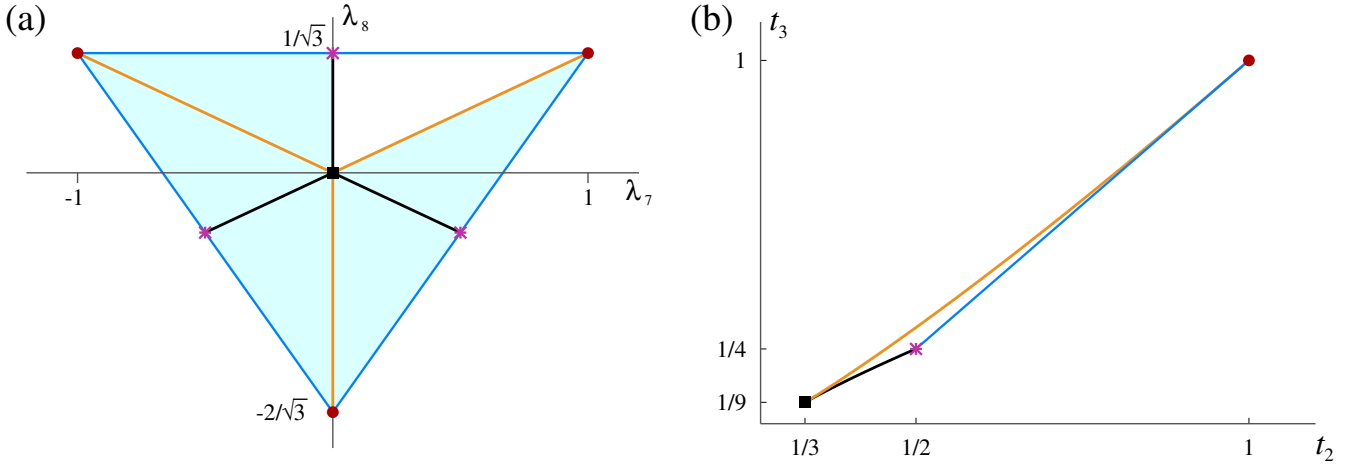


Figure 2. Non-linear map from (a) λ -space to (b) t -space. The pure states (dot-symbol) are mapped onto the vertex \vec{t}_1 (dot-symbol), the middle-points (asterisk-symbol) onto the vertex \vec{t}_2 (asterisk-symbol) and the most mixed state (square-symbol) onto the vertex \vec{t}_3 (square-symbol). Each straight-line segment which connects any two indicated points in λ -space is mapped to a boundary-curve in the t -space, and each open triangle (as the white triangle) is mapped onto the interior of the bounded region in t -space.

and an arbitrary point by

$$\vec{p} \rightarrow \vec{\Lambda} = \left(p_1 - p_2, \frac{1 - 3p_3}{\sqrt{3}}, 1 \right).$$

In figure 1 we show the values which yield a physical state of the system, both in the simplex Fig. 1(a) and the λ -space Fig. 1(b). In both cases the vertices of the triangle correspond to pure states of the system. By considering that the three levels represent an atomic or molecular system and give the level occupation probabilities, we use the following convention: the ground state is indicated by \vec{p}_1 or $\vec{\lambda}_1$ (red dot in the figure), the first excited state by \vec{p}_2 or $\vec{\lambda}_2$ (plus-symbol in the figure), and the second excited state by \vec{p}_3 or $\vec{\lambda}_3$ (times-symbol in the figure).

Other points of interest are the thermal endpoints corresponding to the most mixed state $\vec{p}_e = (\vec{p}_1 + \vec{p}_2 + \vec{p}_3)/3$ or $\vec{\lambda}_e = (\vec{\lambda}_1 + \vec{\lambda}_2 + \vec{\lambda}_3)/3 = (0, 0)$ (square-symbol in the figure), and the cases when two occupation probabilities of the three-level system are equal (i.e., two eigenvalues of the density matrix are degenerate): $\vec{p}_m = (\vec{p}_i + \vec{p}_j)/2$ or $\vec{\lambda}_m = (\vec{\lambda}_i + \vec{\lambda}_j)/2$, $i \neq j$ (asterisk-symbol in the figure).

The open (shaded) internal triangle establishes the case without degeneracy, corresponding to the set of points in the simplex for a thermal density matrix; the black lines connecting the point \vec{p}_e ($\vec{\lambda}_e$) with either the vertex \vec{p}_1 ($\vec{\lambda}_1$) or the middle point \vec{p}_m ($\vec{\lambda}_m$) correspond to trajectories from the pure ground state and from the case of a degenerate ground state with two equal occupation probabilities, respectively. The qualitative behavior of the thermal density matrix as a function of the temperature, for the non-degenerate case, is shown by the black curve in the figure, whose concavity increases when the first excited state occupation probability of the system approaches that of the ground state.

Now, we consider the non-linear map from the λ -space to the t -space (cf. Fig. 2). As pointed out above, this map does not distinguish between pure states, and hence each point in t -space represents a set of physical states. In particular, the pure states $\vec{\lambda}_p$ (dot-symbol) at the vertices, middle points $\vec{\lambda}_m$ (asterisk-symbol), and the most mixed state $\vec{\lambda}_e$ (square-symbol) indicated in Fig. 2(a) are mapped to the points

$$\vec{\lambda}_p \rightarrow \vec{t}_1 = (1, 1); \quad \vec{\lambda}_m \rightarrow \vec{t}_2 = \left(\frac{1}{2}, \frac{1}{4} \right); \quad \vec{\lambda}_e \rightarrow \vec{t}_3 = \left(\frac{1}{3}, \frac{1}{9} \right),$$

indicated with the same symbols in Fig. 2(b). Any point $\vec{\lambda} = (\lambda_7, \lambda_8)$ in λ -space is mapped to a point $\vec{t} = (t_2, t_3)$ via the transformation

$$\vec{\lambda} \rightarrow \vec{t} = \left(\frac{1}{3} + \frac{1}{2} (\lambda_7^2 + \lambda_8^2), \frac{1}{9} + \frac{\lambda_7^2}{4} (2 + \sqrt{3}\lambda_8) + \frac{\lambda_8^2}{4\sqrt{3}} (2\sqrt{3} - \lambda_8) \right).$$

The straight line segments connecting points in the λ -space, shown in Fig. 2(a), can be parametrized as follows:

$$\vec{\lambda}_j^{ep} = \vec{\lambda}_j x; \quad \vec{\lambda}_{jk}^{em} = \frac{1}{2} (\vec{\lambda}_j + \vec{\lambda}_k) x; \quad x \in [0, 1],$$

$$\vec{\lambda}_{jk}^{mp} = \vec{\lambda}_j + (\vec{\lambda}_k - \vec{\lambda}_j) x; \quad x \in \left[\frac{1}{2}, 1 \right],$$

for $j, k = 1, 2, 3$, with the upper-indices indicating the corresponding connected points: most mixed state (e), middle point of two occupation probabilities (m), and pure states (p). Each path maps onto a trajectory in t -space corresponding to their boundaries. Any point in t -space lying within these trajectories is physically acceptable (and only those), since the density matrix is given in a diagonal form. After the transformation these segments will be given by (see Fig. 2(b))

$$\vec{t}_1^{ep} = \frac{1}{9} (3 + 6x^2, 1 + 6x^2 + 2x^3); \quad x \in [0, 1],$$

$$\vec{t}_{12}^{em} = \frac{1}{3} \left(1 + \frac{x^2}{2}, \frac{1}{3} + \frac{x^2}{2} - \frac{x^3}{12} \right); \quad x \in [0, 1],$$

$$\vec{t}_{21}^{mp} = (1 - 2x + 2x^2, 1 - 3x + x^2); \quad x \in \left[\frac{1}{2}, 1 \right].$$

Notice that the open internal triangle in the λ -space [white triangle in Figure 2(a)], representing the domain of thermal states as was discussed previously [cf. Figs. 1(b) and 2(a)], is mapped onto the full open region in t -space bounded by the trajectories shown. In fact, all points \vec{t} with exception of the boundary that connects the vertices \vec{t}_1 and \vec{t}_2 may be associated to a thermal state. The same happens for all other triangles in the λ -space.

The non-linear map from the Gell-Mann variables to the invariants representation has been given above; however it is interesting to determine the set of density matrices with equal invariants, i.e., the set with equal $t_2 = \text{Tr}[\rho^2]$ (purity), or with $t_3 = \text{Tr}[\rho^3]$ a constant value. The first condition $p_1^2 + p_2^2 + p_3^2 = t_2$ gives a circumference centered at \vec{p}_e on the simplex, which can be parametrized by

$$\vec{p}_{t_2} = \vec{p}_e + \sqrt{\frac{3t_2 - 1}{3}} (\mathbf{p}_{1e} \cos(\alpha) + \mathbf{q}_{1e} \sin(\alpha)); \quad \alpha \in [0, 2\pi], \quad (30)$$

with the constraint

$$\frac{1}{3} \leq t_2 \leq 1,$$

and where we have chosen the unit vectors

$$\mathbf{p}_{1e} := \frac{\vec{p}_1 - \vec{p}_e}{\|\vec{p}_1 - \vec{p}_e\|}; \quad \mathbf{q}_{1e} := \frac{\vec{p}_e \times \vec{p}_1}{\|\vec{p}_e \times \vec{p}_1\|}.$$

The case t_3 constant is given by the set of points of the form

$$\vec{p}_{t_3} = \vec{p}_e + r(t_3, \alpha) (\mathbf{p}_{1e} \cos(\alpha) + \mathbf{q}_{1e} \sin(\alpha)); \quad \alpha \in [0, 2\pi], \quad (31)$$

where $r(t_3, \alpha)$ satisfies

$$\frac{1}{9} + r^2 + \frac{\cos(3\alpha)}{\sqrt{6}} r^3 = t_3,$$

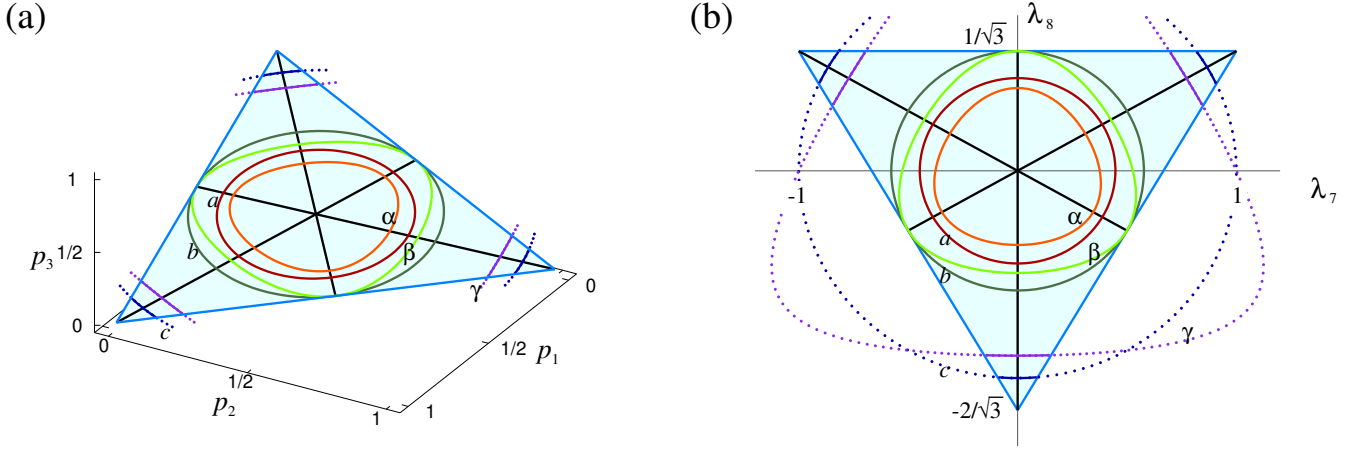


Figure 3. Simplex in the p -space (a), and affine λ -space (b). The edges of the simplex given by Eq. (25) correspond to states with at least one eigenvalue equal to zero; the medians of the triangle given by Eq. (26) contain states with at least two eigenvalues equal to zero; the centered circles given by Eq. (30) represent the set of density matrices with equal purity (invariant t_2), shown for the values $t_2 = 13/30, 1/2, 5/6$ (labeled by a , b and c , respectively); while the triangles with rounded vertices given by Eq. (31) represent the set of density matrices with fixed invariant t_3 , here shown for the values $t_3 = 109/600, 1/4, 11/18$ (labeled by α , β and γ , respectively). The corresponding ones, via the linear transformation, are shown at right in the λ -space.

and the constraints for having physical states are

$$\frac{1}{9} \leq t_3 \leq 1, \quad 0 \leq r \leq \sqrt{\frac{2}{3}}.$$

The latter are obtained by using the boundaries of the invariant t_2 and the fact that r is the radius in a polar coordinate vector representation, so that \vec{p}_{t_3} is a single-valued vector function of α . Additional to these constraints, we know that only the points of the simplex represent physical states, i.e., $p_1 + p_2 + p_3 = 1$.

In the λ -space the same set of trajectories are obtained from the linear map $\vec{\Lambda} = \mathbf{M}^{-1}\vec{p}$ with \mathbf{M} given in Eq. (29). So the parametric curves in the λ -space read: $\vec{\Lambda}_{jk} = \mathbf{M}^{-1}\vec{p}_{jk}$, $\vec{\Lambda}_{jkl} = \mathbf{M}^{-1}\vec{p}_{jkl}$, $\vec{\Lambda}_{t_2} = \mathbf{M}^{-1}\vec{p}_{t_2}$ and $\vec{\Lambda}_{t_3} = \mathbf{M}^{-1}\vec{p}_{t_3}$, respectively.

In figure 3, one can see all the characteristics mentioned above for the qutrit system in the p -space, Fig. 3(a), and in the λ -space, Fig. 3(b). The edges of the simplex given by Eq. (25) represent the set of density matrices with at least one of their eigenvalues equal to zero; the medians of the triangle (black lines) parametrized by Eq. (26) correspond to the set of density matrices with at least two degenerate eigenvalues; the curves (or segments of curve thereof) inside the simplex represent the set of states with one invariant constant. For t_2 , corresponding to circles with center at the most mixed state Eq. (30), we have labeled a few cases: (a) for $t_2 = 13/30$, (b) for $t_2 = 1/2$, and (c) for $t_2 = 5/6$. For t_3 constant Eq. (31) we have trajectories that look like triangles with rounded vertices (resembling a Reuleaux triangle) centered at the most mixed state, and we have labeled: (α) for $t_3 = 109/600$, (β) for $t_3 = 1/4$, and (γ) for $t_3 = 11/18$. In both cases we may see the continuation out the simplex (unphysical states) of the broken trajectories, drawn with dots, in order to illustrate the shape of the full curve in the whole space.

Now for the non linear map from the λ -space to the t -space. The centered circumferences in the λ -space or p -space map onto vertical cutoff lines in the t -space, while the kind of trajectories given by

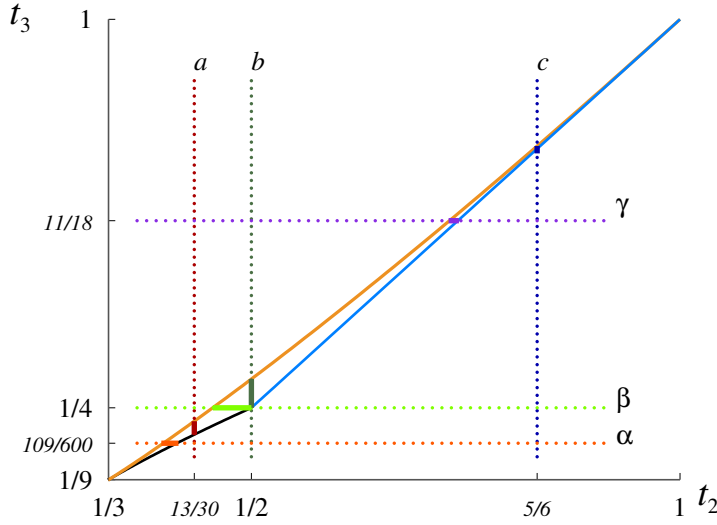


Figure 4. Physical region in t -space obtained via the non-linear map from the simplex in the p -space or the affine domain in the λ -space [Eqs. (25)–(31)]. The image of the curves in Figure 3 carry the same labels here. The unphysical states along the constant dotted lines are drawn for the purpose of clarity. The boundary of the region is given by $t_3 = t_2 - \frac{2}{9} \pm \frac{(3t_2-1)^{3/2}}{9\sqrt{2}}$, (upper (orange) and short lower (black) lines respectively) and are associated to density matrices with two equal eigenvalues, while the long lower (blue) curve is described by $t_3 = \frac{1}{2}(3t_2 - 1)$ and is associated to density matrices with an eigenvalue equal to zero.

Eq. (31), which resemble a kind of Reuleaux triangle, map onto horizontal cutoff lines in the t -space. These are shown in Figure 4, where we have labeled the trajectories in a similar fashion to Figure 3. For clarity, we have extended the trajectories out of the physical region with dotted lines; the counterpart to these extensions, which are unphysical, do not appear in the non-linear map of a single inscribed curve in the affine domain of the λ -space, since any inscribed curve in the affine domain maps to a curve in the physical t -space. The boundary of the compact region in Figure 4 corresponds to the edges and medians of the triangle (see Fig. 2), i.e., they are composed by states with at least one vanishing eigenvalue (vertices and edges of the triangle in the p - or λ -space) and states with degenerate eigenvalues (medians of the triangle in the p - or λ -space).

Summarizing, we have represented a qutrit by a 3×3 matrix yielding three eigenvalues in its diagonal representation, i.e., $\rho_D = \text{DiagM}(p_1, p_2, p_3)$. The diagonal state can be studied in several ways, by examining directly the three eigenvalues (p -space), equivalently in a 2-dimensional λ -space by using the Gell-Mann parametrization, or by exploring the invariants of the density matrix $t_2 = \text{Tr } \rho_D^2$ and $t_3 = \text{Tr } \rho_D^3$ (t -space).

3.2. Ququart system

The diagonal density matrix of a ququart system is given in p -space as Eq. (20)

$$\rho = \text{DiagM}(p_1, p_2, p_3, p_4) = \text{DiagM}(\vec{p}),$$

its 3-simplex in $U(4)$ is a tetrahedron with vertices at $\rho_j = \text{DiagM}(\vec{p}_j)$ for which $p_j = 1$. It can be visualized as a solid in 3-dimensional space, generated by the probabilities p_2, p_3 and p_4 , with $p_1 = 1 - p_2 - p_3 - p_4$ as in figure 5(a). Its vertices, indicated by dot-, square-, plus- and times-symbols, correspond to pure states; according to $\rho_j = \text{DiagM}(\vec{p}_j)$ these are denoted by ρ_1, ρ_2, ρ_3 and ρ_4 . The

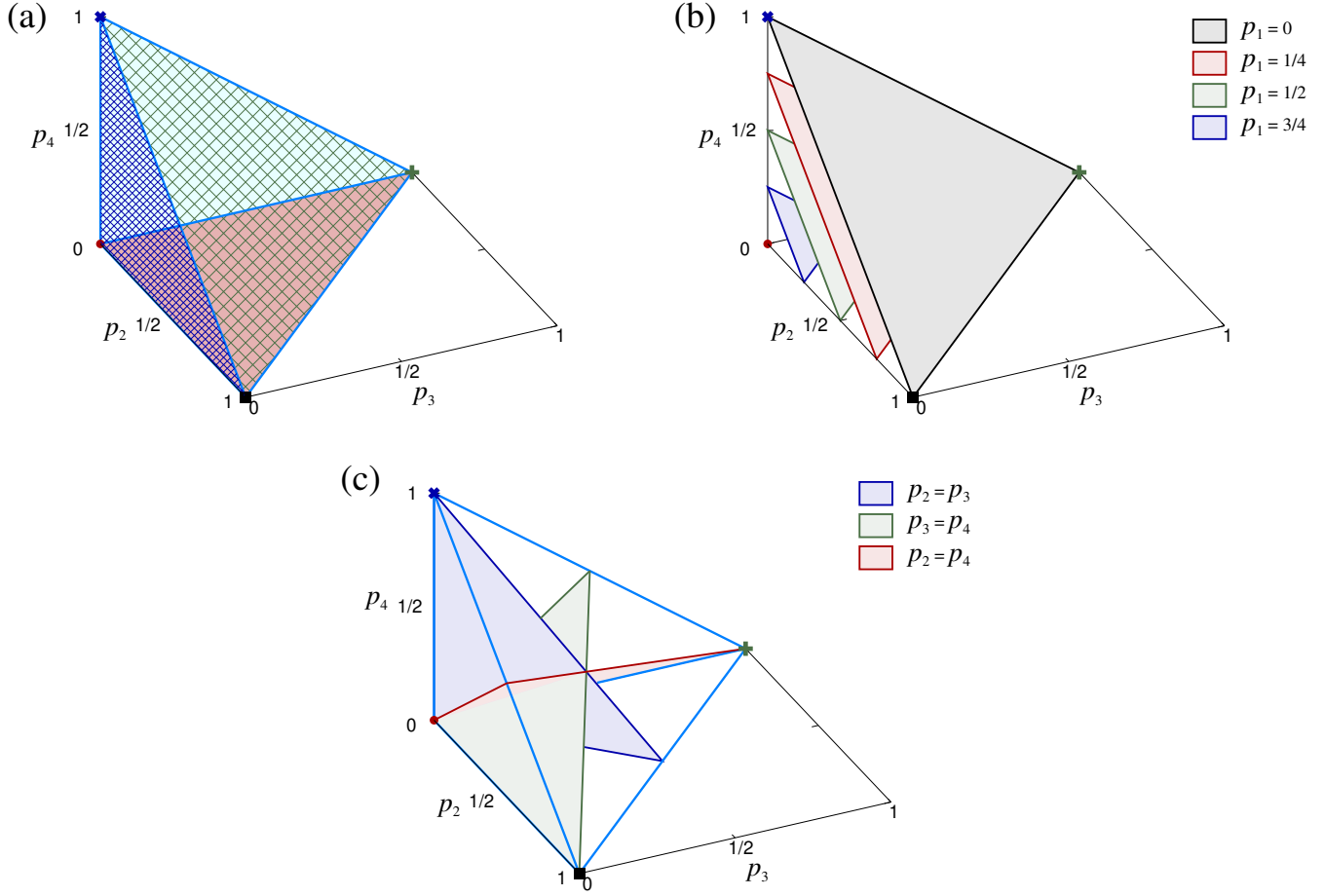


Figure 5. Simplex for a ququart system in p -space. (a) Solid region in the subspace $\{p_2, p_3, p_4\}$; (b) the simplex for fixed values of probability p_1 ; and (c) the cut planes when two probabilities take the same value. In all cases the pure states are indicated by dot-symbols for ρ_1 , square-symbols for ρ_2 , plus-symbols for ρ_3 and times-symbols for ρ_4 .

faces correspond to the set of points where at least one eigenvalue is zero, while at the edges at least two eigenvalues vanish. Therefore one has double degeneracy corresponding (as a limit case, see discussion below) to the orbits in $U(4)$ of dimension 6, associated to the quotient group $U(4)/(U(2) \otimes U(1) \otimes U(1))$. For a fixed value of p_1 the set given by

$$p_2 + p_3 + p_4 = c \geq 0; \quad c := 1 - p_1,$$

defines a region similar to that in the case of the qutrit [cf. Fig. 1(a)] which grows as $p_1 \rightarrow 0$ (cf. Fig. 5(b)). The case when two probability values are equal, given by the condition

$$p_j + p_k + 2p_\ell = 1, \quad p_m = p_\ell,$$

cuts the simplex at a plane; the cases $p_m = p_\ell$ with $m \neq 1$ and $\ell \neq 1$ are shown in figure 5(c). These planes in turn generate the medians of the triangular face for a constant value p_1 . The most mixed state is given by the point

$$\vec{p}_e := \frac{1}{4}(1, 1, 1, 1).$$

Using this, one may parametrize each point of the simplex in the p -space as

$$\vec{p} = \vec{p}_e + \frac{r}{\sqrt{2}} [\cos(\phi) \sin(\theta) \hat{e}_1 + \sin(\phi) \sin(\theta) \hat{e}_2 + \cos(\theta) \hat{e}_3], \quad (32)$$

with $r \geq 0, \phi \in [0, 2\pi]$ and $\theta \in [0, \pi]$ and where the unitary vectors are given by

$$\begin{aligned}\hat{e}_1 &= \frac{1}{\sqrt{2}}(1, -1, 0, 0); & \hat{e}_2 &= \frac{1}{\sqrt{6}}(1, 1, -2, 0); \\ \hat{e}_3 &= \frac{\sqrt{3}}{6}(1, 1, 1, -3).\end{aligned}$$

The advantage of writing the point in the simplex in this form is to obtain the invariants in terms of the radial and polar variables, so a density matrix which is written in a general form as $\rho = \text{DiagM}(\vec{p})$ has the invariants written simply as

$$\begin{aligned}t_2 &= \frac{1}{4}(1 + 2r^2); & t_3 &= \frac{1}{16} + \frac{3}{8}r^2 + \frac{a_3}{96}r^3; \\ t_4 &= \frac{1}{64} + \frac{3}{16}r^2 + \frac{a_3}{96}r^3 + \frac{b_4}{384}r^4,\end{aligned}\tag{33}$$

where we have used

$$\begin{aligned}a_3 &:= -\sqrt{6}[3\cos(\theta) + 5\cos(3\theta)] + 8\sqrt{3}\sin^3(\theta)\sin(3\phi); \\ b_4 &:= 45 + 4\cos(2\theta) + 7\cos(4\theta) + 32\sqrt{2}\cos(\theta)\sin^3(\theta)\sin(3\phi),\end{aligned}$$

to simplify the notation. Thus, in the p -space the condition t_2 constant yields a hyper-sphere of radius $r = \sqrt{4t_2 - 1}/2$ centred at \vec{p}_e . On the simplex, represented by the coordinate axes p_2, p_3 and p_4 , this hyper-sphere is seen elongated: at the limit values of t_2 one obtains the point \vec{p}_e ($t_2 = 1/4$) and a surface which intersects the simplex only at the vertices ($t_2 = 1$); intermediate values generate a surface lying completely inside the simplex. Figure 6 shows this for different values of t_2 : (a) $t_2 = 1/3$; (b) $t_2 = 1/2$. Points outside the simplex correspond to unphysical states.

Solving for t_3 and t_4 in terms of $r \geq 0$ one finds the parametric form of the surfaces of constant value for each of the invariants. In both cases one has a symmetry of $2\pi/3$ in the angular variable ϕ as expected by the form of the coefficients a_3 and b_4 . These surfaces are shown in Figure 6, (c) for $t_3 = 1/10$, (d) for $t_3 = 7/40$, (e) for $t_4 = 1/32$ and (f) for $t_4 = 5/64$.

The explicit density matrix in the λ -space can be written as

$$\rho = \text{DiagM}\left(\frac{1}{4} + \frac{\lambda_{13}}{2} + \frac{\lambda_{14}}{2\sqrt{3}} + \frac{\lambda_{15}}{2\sqrt{6}}, \frac{1}{4} - \frac{\lambda_{13}}{2} + \frac{\lambda_{14}}{2\sqrt{3}} + \frac{\lambda_{15}}{2\sqrt{6}}, \frac{1}{4} - \frac{\lambda_{14}}{\sqrt{3}} + \frac{\lambda_{15}}{2\sqrt{6}}, \frac{1}{4} - \frac{3\lambda_{15}}{2\sqrt{6}}\right).\tag{34}$$

Since the density matrix is positive semi-definite $0 \leq \rho_{jj} \leq 1$ ($j = 1, \dots, 4$), we have a tetrahedron given by

$$-1 \leq \lambda_{13} \leq 1, \quad -\frac{2}{\sqrt{3}} \leq \lambda_{14} \leq \frac{1}{\sqrt{3}}, \quad -\sqrt{\frac{2}{3}} \leq \lambda_{15} \leq \frac{1}{\sqrt{6}}.\tag{35}$$

The pure states, corresponding to the density matrices $\rho = \text{diag}(1, 0, 0, 0)$, $\rho = \text{diag}(0, 1, 0, 0)$, $\rho = \text{diag}(0, 0, 1, 0)$, and $\rho = \text{diag}(0, 0, 0, 1)$, are associated to the vertices $(1, \frac{1}{\sqrt{3}}, \frac{1}{\sqrt{6}})$, $(-1, \frac{1}{\sqrt{3}}, \frac{1}{\sqrt{6}})$, $(0, -\frac{2}{\sqrt{3}}, \frac{1}{\sqrt{6}})$, and $(0, 0, -\sqrt{\frac{2}{3}})$, respectively. The values for λ_{13} , λ_{14} , λ_{15} on the faces of the tetrahedron correspond to pure states, while the centroid corresponds to the most mixed state with $\rho = \text{diag}(1/4, 1/4, 1/4, 1/4)$.

To visualise the thermal region it is convenient to consider the Gell-Mann representation, by choosing the diagonal matrices as

$$\begin{aligned}\Lambda_{13} &= \text{DiagM}(1, -1, 0, 0); & \Lambda_{14} &= \frac{1}{\sqrt{3}}\text{DiagM}(1, 1, -2, 0); \\ \Lambda_{15} &= \frac{1}{\sqrt{6}}\text{DiagM}(1, 1, 1, -3);\end{aligned}$$

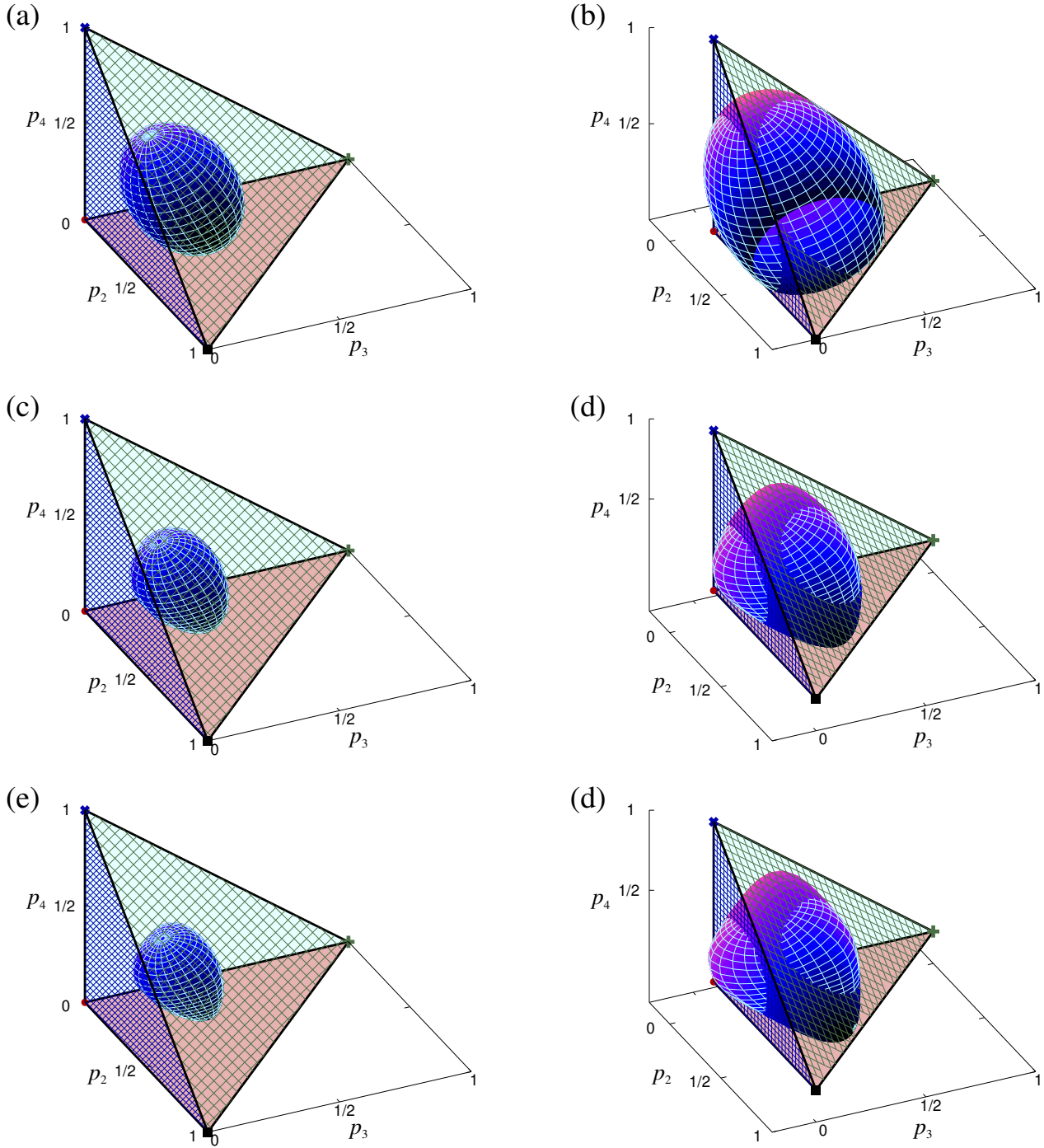


Figure 6. Surfaces defined on the 3-simplex for the ququart when the invariants of $SU(4)$ take a constant value: (a) $t_2 = 1/3$, (b) $t_2 = 1/2$, (c) $t_3 = 1/10$, (d) $t_3 = 7/40$ (e) $t_4 = 1/32$ and (f) $t_4 = 5/64$. Points outside the simplex correspond to unphysical states.

each point $\vec{\Lambda} := (\lambda_{13}, \lambda_{14}, \lambda_{15}, 1)$ is related to the vector $\vec{p} = (p_1, p_2, p_3, p_4)$ in probability space via the linear map

$$\vec{p} = \mathbf{M}\vec{\Lambda}; \quad \vec{\Lambda} = \mathbf{M}^{-1}\vec{p}$$

where the matrix transformation is

$$\mathbf{M} = \frac{1}{2} \begin{pmatrix} 1 & \frac{1}{\sqrt{3}} & \frac{1}{\sqrt{6}} & \frac{1}{2} \\ -1 & \frac{1}{\sqrt{3}} & \frac{1}{\sqrt{6}} & \frac{1}{2} \\ 0 & -\frac{2}{\sqrt{3}} & \frac{1}{\sqrt{6}} & \frac{1}{2} \\ 0 & 0 & -\sqrt{\frac{3}{2}} & \frac{1}{2} \end{pmatrix}; \quad \mathbf{M}^{-1} = \begin{pmatrix} 1 & -1 & 0 & 0 \\ \frac{1}{\sqrt{3}} & \frac{1}{\sqrt{3}} & -\frac{2}{\sqrt{3}} & 0 \\ \frac{1}{\sqrt{6}} & \frac{1}{\sqrt{6}} & \frac{1}{\sqrt{6}} & -\sqrt{\frac{3}{2}} \\ 1 & 1 & 1 & 1 \end{pmatrix},$$

and the λ -space is defined by the points of the form $\vec{\lambda} = (\lambda_{13}, \lambda_{14}, \lambda_{15})$.

From Eq.(32) where the unit vectors \hat{e}_j are defined to parametrize the probability vector \vec{p} , and the relation between the latter and the diagonal Gell-Mann matrices Λ_{jk} , it is clear that any hypersurface t_2 constant is mapped to a sphere in the λ -space. The affine space of states in the λ -space is a tetrahedron which is shown in Figure 7(a), where the vertices correspond to pure states indicated by dot-, plus-, times-, and square-symbols respectively. Under the map these are

$$\begin{aligned} \vec{p}_1 \rightarrow \vec{\lambda}_1 &= \left(1, \frac{1}{\sqrt{3}}, \frac{1}{\sqrt{6}}\right); & \vec{p}_2 \rightarrow \vec{\lambda}_2 &= \left(-1, \frac{1}{\sqrt{3}}, \frac{1}{\sqrt{6}}\right); \\ \vec{p}_3 \rightarrow \vec{\lambda}_3 &= \left(0, -\frac{2}{\sqrt{3}}, \frac{1}{\sqrt{6}}\right); & \vec{p}_4 \rightarrow \vec{\lambda}_4 &= \left(0, 0, -\sqrt{\frac{3}{2}}\right), \end{aligned}$$

which yield the limit values of $\vec{\lambda}$ for physical states. Referring to this figure, we may visualize the thermal states by assigning a definite meaning to each vertex; thus, we choose p_1 to denote the probability of the ground state (dot-symbol), p_2 for the probability of the first excited state (plus-symbol), p_3 for that of the second excited state (times-symbol), and p_4 for that of the third excited state (square-symbol). This would give the condition $p_1 \geq p_2 \geq p_3 \geq p_4$. The planes defined by $p_1 = p_2$, $p_2 = p_3$ and $p_3 = p_4$ are mapped onto planes in the λ -space and the intersection with the affine space of states provides the faces of the thermal region shown in Fig. 7(b). In this sense, with the exception of the upper face, each point in this region is related to a density matrix of the form Eq. (7). As mentioned before, for infinite temperature the thermal state corresponds to the most mixed state, indicated by an empty triangle-symbol, and for zero temperature the thermal state corresponds to a ground state (dot-symbol) without degeneracy; the case for the ground state with degeneracy is indicated by a triangle-symbol (degeneracy of order two) and empty square-symbol (degeneracy of order three), respectively. So, the thermal state as a function of the temperature moves along a trajectory which connects the most mixed state with one of the other three end points depending of the degeneracy of the system. Fig. 7(c) shows these paths: a solid black line for the general case without degeneracy, while for the degenerate cases the path lies on a face or edge of the affine space; for example, for values $p_1 = p_2$ with $p_3 \neq p_1$ and $p_3 \neq p_4$ the trajectory is over the face $\lambda_{13} = 0$ (drawn with a dashed-line for $p_3 \approx p_4$, and with a short-dashed-line for $p_3 \approx p_1$). A similar behavior is had on the other thermal faces defined by the degeneracy $p_2 = p_3$ and $p_3 = p_4$, with the trajectories on the edges corresponding to the cases for double degeneracy $p_1 = p_2$ and $p_3 = p_4$ (dotted-line), degeneracy of order three $p_1 = p_2 = p_3$ (dashed-line), and when $p_2 = p_3 = p_4$ (dash-dot-line).

Finally, for $\vec{\lambda} = r(\cos(\phi)\sin(\theta), \sin(\phi)\sin(\theta), \cos(\theta))$ in spherical coordinates, the non-linear map from λ -space to the invariants t -space $\vec{\lambda} \rightarrow \vec{t} = (t_2, t_3, t_4)$ gives us the values t_j shown by Eq. (33). The

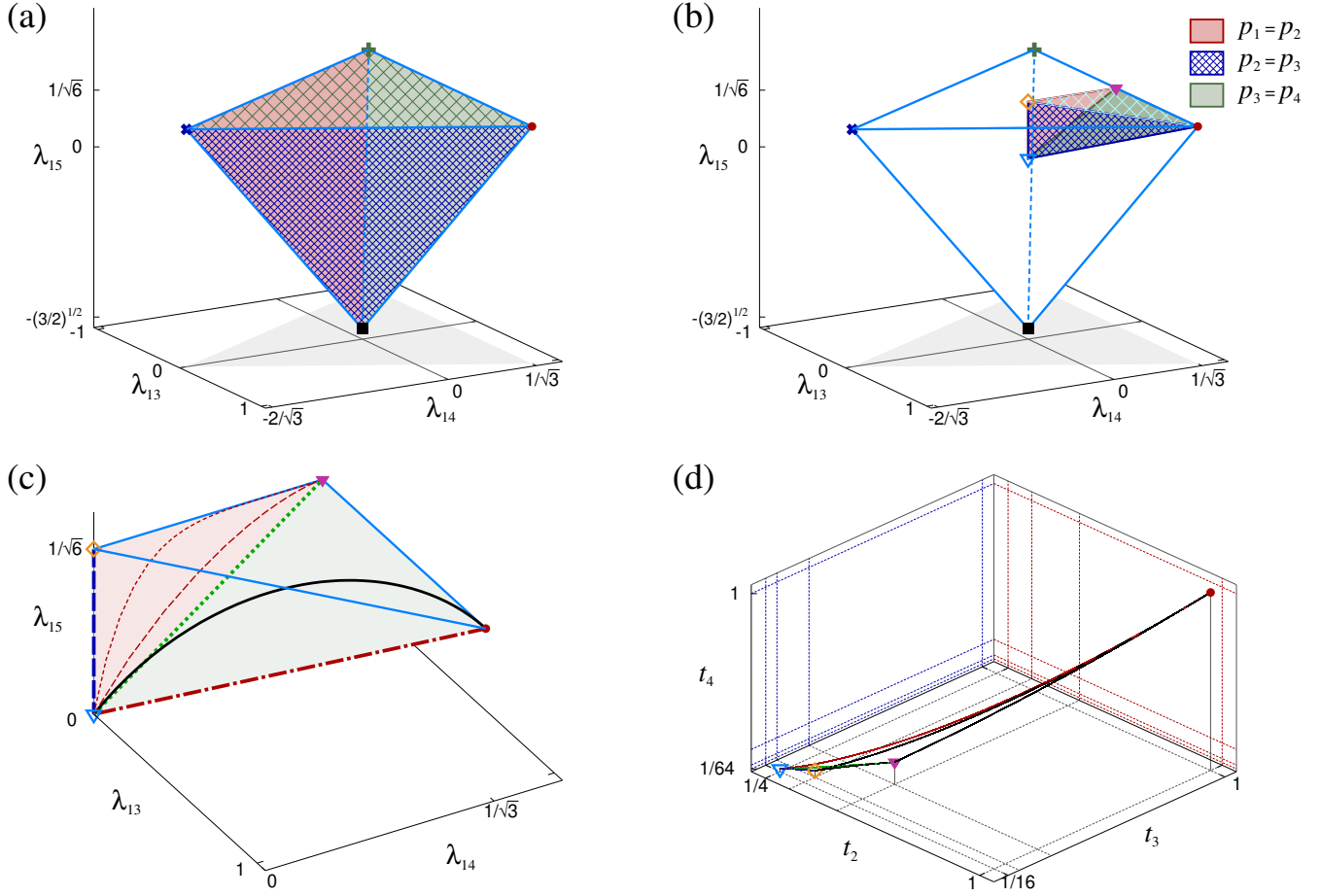


Figure 7. (a) Simplex for a ququart system in the λ -space. (b) Thermal state region by choosing the vertices to represent probabilities for ground state (dot-symbol), first excited state (plus-symbol), second excited state (times-symbol) and third excited state (square-symbol). Other points indicated are for the most entangled state (empty triangle-symbol), the end point for degeneracy $p_1 = p_2$ (solid triangle-symbol) and the end point for degeneracy $p_1 = p_2 = p_3$ (empty square-symbol). (c) Zoom-in of the thermal states region with some trajectories as functions of the temperature. (d) The physical states region in t -space obtained from the non-linear map applied to the thermal region in λ -space. See text for details.

end points of the thermal region are mapped to the vertices of the physical region in the t -space [cf. Eq. (24)], i.e., these points are representative of a particular kind of states in t -space. In the λ -space these points are given by $\vec{\lambda}_p = (1, 1/\sqrt{3}, 1/\sqrt{6})$ (ground state), $\vec{\lambda}_{12} = (0, 1/\sqrt{3}, 1/\sqrt{6})$ (the degenerate case $p_1 = p_2$), $\vec{\lambda}_{123} = (0, 0, 1/\sqrt{6})$ (the degenerate case $p_1 = p_2 = p_3$) and $\vec{\lambda}_e = (0, 0, 0)$ (the most entangled state), and these are mapped to $\vec{\lambda}_p \rightarrow \vec{t}_1$, $\vec{\lambda}_{12} \rightarrow \vec{t}_2$, $\vec{\lambda}_{123} \rightarrow \vec{t}_3$ and $\vec{\lambda}_e \rightarrow \vec{t}_4$; these points together with the boundary of the thermal state region are shown in Fig. 7(d).

4. Thermal states

The different diagonal representations discussed above allow us to study several processes related to three- and four-level systems. For example, one may study the thermodynamics of the Gibbs states represented by Eq. (7) for different Hamiltonians. In this section, we present the study for two cases: where the Hamiltonian is given as a linear form of the angular momentum generators \mathbf{J}_x , \mathbf{J}_y , and \mathbf{J}_z ;

and in the quadratic form described by the LMG Hamiltonian model.

4.1. Linear Hamiltonian

The linear Hamiltonian can be written as

$$H = \omega \hat{n} \cdot \mathbf{J}, \quad (36)$$

where $\hat{n} = (\sin \theta \cos \phi, \sin \theta \sin \phi, \cos \theta)$ denotes the unit vector in spherical coordinates. By means of the basis states of \mathbf{J}^2 and \mathbf{J}_n denoted by $|J, M\rangle_n$ the eigenvectors and eigenvalues are given by the expressions ($\hbar = 1$)

$$E_M = \omega M; \quad |J, M\rangle_n = \sum_{\mu=-J}^J D_{\mu,M}^J(0, -\theta, \phi) |J, \mu\rangle, \quad (37)$$

with $M = -J, -J+1, \dots, J-1, J$, and $D_{\mu,M}^J$ indicating the Wigner rotational matrix.

For this system, the PME of an ensemble of particles of spin \mathbf{J} and with a well defined mean value of the energy yields a density matrix of the form (cf. Section 2)

$$\rho = \text{Diag} (p_1, p_2, \dots, p_{2J}, p_{2J+1}) , \quad (38)$$

with

$$p_M = \frac{e^{-\beta E_M}}{\sum_{M=-J}^J e^{-\beta E_M}}. \quad (39)$$

The expressions (38) and (39) will be used to describe the thermal state of a qutrit with $J = 1$ and that of a ququart with $J = 3/2$. The qutrit corresponding to a 3-level system has equidistant energy levels $E_1 = -\omega$, $E_2 = 0$ and $E_3 = \omega$, and occupation probabilities

$$p_1 = \frac{e^{-\beta \omega}}{1 + 2 \cosh(\beta \omega)}, \quad p_2 = \frac{1}{1 + 2 \cosh(\beta \omega)}, \quad p_3 = \frac{e^{\beta \omega}}{1 + 2 \cosh(\beta \omega)}. \quad (40)$$

Notice that one gets the same results by considering the matrix Hamiltonian in the basis states of \mathbf{J}^2 and \mathbf{J}_z , where its matrix elements depend on the spherical angles (θ, ϕ) . After the construction of the Boltzmann density matrix is done, its eigenvalues will of course correspond to the occupation probabilities given above.

In the vicinity of the most mixed state ($\beta \omega$ small) the occupation probabilities of the Boltzmann distribution are linear functions of the energy, i.e.,

$$p_1 \approx \frac{1}{3}(1 - \beta \omega), \quad p_2 \approx \frac{1}{3}, \quad p_3 \approx \frac{1}{3}(1 + \beta \omega). \quad (41)$$

The dependency between the variables t_2 and t_3 can be seen in Figure 8 (left). The curve defined by the thermal states crosses the allowed region to define a valid quantum system, from the most mixed state ($t_2 = 1/3, t_3 = 1/9$) to the pure state state ($t_2 = t_3 = 1$), which are reached when the temperature of the system is $T \rightarrow \infty$ and $T \rightarrow 0$, respectively (as mentioned above).

The occupation probabilities (40) satisfy

$$p_2^2 = p_1 p_3, \quad (42)$$

and the invariants of the density matrix take the form

$$t_1 = 1, \quad t_2 = \frac{2 \cosh(\beta \omega) - 1}{1 + 2 \cosh(\beta \omega)}, \quad t_3 = \frac{1 + 2 \cosh(3 \beta \omega)}{(1 + 2 \cosh(\beta \omega))^3}; \quad (43)$$

they are not independent, as

$$t_3 = \frac{1}{8} (9t_2^2 - 3t_2^3 + 3t_2 - t_1), \quad (44)$$

shown by the interior (red) curve in Figure 8 (left).

Since the labeling of the energy levels of the system is arbitrary, we may take all their possible permutations arriving at the three possible curves

$$p_1^2 = p_2 p_3, \quad p_2^2 = p_1 p_3, \quad p_3^2 = p_1 p_2. \quad (45)$$

These curves follow a three-petal-flower-like structure as shown in Figure 8 (right).

The probabilities allow us to obtain the Gell-Mann parameters

$$\lambda_7 = \frac{1 - e^{-\beta\omega}}{1 + 2 \cosh(\beta\omega)}, \quad \lambda_8 = \frac{1 - 3 \sinh(\beta\omega) - \cosh(\beta\omega)}{\sqrt{3}(1 + 2 \cosh(\beta\omega))}. \quad (46)$$

By using the expressions in Eq. (45) together with (46) and the relation between the λ parameters and the probabilities $p_1 = \frac{\lambda_7}{2} + \frac{\lambda_8}{2\sqrt{3}} + \frac{1}{3}$, $p_2 = -\frac{\lambda_7}{2} + \frac{\lambda_8}{2\sqrt{3}} + \frac{1}{3}$, and $p_3 = \frac{1}{3} - \frac{\lambda_8}{\sqrt{3}}$ one arrives at the following curves in λ -space

$$3\lambda_7(\lambda_7 \pm 2) + \lambda_8(3\lambda_8 + 2\sqrt{3}) = 0, \quad 3\lambda_7^2 + \lambda_8(3\lambda_8 - 4\sqrt{3}) = 0. \quad (47)$$

The curves follow the same flower-like structure as in the case of the probabilities [see Figure 8 (bottom)].

4.2. Ququart

For the four-level system the thermal state is given by the following density matrix

$$\rho = \begin{pmatrix} f_-^3 \sinh\left(\frac{\eta}{2}\right) \text{csch}(2\eta) & -\frac{\sqrt{3}}{4} f_-^2 n_- \tanh\left(\frac{\eta}{2}\right) \text{sech}(\eta) & \sqrt{3} f_- n_-^2 \sinh^3\left(\frac{\eta}{2}\right) \text{csch}(2\eta) & -n_-^3 \sinh^4\left(\frac{\eta}{2}\right) \text{csch}(2\eta) \\ -\frac{\sqrt{3}}{4} f_-^2 n_+ \tanh\left(\frac{\eta}{2}\right) \text{sech}(\eta) & \frac{1}{8} f_- g_- \text{sech}\left(\frac{\eta}{2}\right) & -\frac{1}{8} g_+ n_- \tanh\left(\frac{\eta}{2}\right) & \sqrt{3} f_+ n_-^2 \sinh^3\left(\frac{\eta}{2}\right) \text{csch}(2\eta) \\ \sqrt{3} f_- n_+^2 \sinh^3\left(\frac{\eta}{2}\right) \text{csch}(2\eta) & -\frac{1}{8} g_+ n_+ \tanh\left(\frac{\eta}{2}\right) & \frac{1}{8} f_+ g_- \text{sech}\left(\frac{\eta}{2}\right) & -\frac{\sqrt{3}}{4} f_+^2 n_- \tanh\left(\frac{\eta}{2}\right) \text{sech}(\eta) \\ -n_+^3 \sinh^4\left(\frac{\eta}{2}\right) \text{csch}(2\eta) & \sqrt{3} f_+ n_+^2 \sinh^3\left(\frac{\eta}{2}\right) \text{csch}(2\eta) & -\frac{\sqrt{3}}{4} f_+^2 n_+ \tanh\left(\frac{\eta}{2}\right) \text{sech}(\eta) & f_+^3 \sinh\left(\frac{\eta}{2}\right) \text{csch}(2\eta) \end{pmatrix} \quad (48)$$

where $\eta = \beta\omega$, $n_{\pm} = n_x \pm i n_y$, $f_{\pm} = \cosh\left(\frac{\eta}{2}\right) \pm \cos(\theta) \sinh\left(\frac{\eta}{2}\right)$, $g_{\pm} = 3 \sin^2(\theta) + (3 \cos^2(\theta) \pm 1) \text{sech}(\eta)$. Associated to this thermal state the invariants t_2 , t_3 , and t_4 , are equal to

$$\begin{aligned} t_2 &= \frac{1}{4} \left(4 - \text{sech}^2\left(\frac{\beta\omega}{2}\right) - 2 \text{sech}(\beta\omega) \right), \\ t_3 &= 1 - \frac{3}{8(\cosh(\beta\omega) + 1)} + \frac{3 \text{sech}(\beta\omega)}{8} (\text{sech}(\beta\omega) - 3), \\ t_4 &= \frac{1}{128} (\cosh(2\beta\omega) + \cosh(6\beta\omega)) \text{sech}^4\left(\frac{\beta\omega}{2}\right) \text{sech}^4(\beta\omega). \end{aligned} \quad (49)$$

The probabilities can be expressed as follows

$$\begin{aligned} p_1 &= \frac{\sinh\left(\frac{3\omega\beta}{2}\right) + \cosh\left(\frac{3\omega\beta}{2}\right)}{2 \left(\cosh\left(\frac{\omega\beta}{2}\right) + \cosh\left(\frac{3\omega\beta}{2}\right) \right)}, & p_2 &= \frac{\left(\tanh\left(\frac{\omega\beta}{2}\right) + 1 \right) \text{sech}^2\left(\frac{\omega\beta}{2}\right)}{4 \left(\tanh^2\left(\frac{\omega\beta}{2}\right) + 1 \right)}, \\ p_3 &= \frac{\text{sech}^4\left(\frac{\omega\beta}{2}\right)}{4 \left(\tanh\left(\frac{\omega\beta}{2}\right) + 1 \right) \left(\tanh^2\left(\frac{\omega\beta}{2}\right) + 1 \right)}, & p_4 &= \frac{\text{sech}^6\left(\frac{\omega\beta}{2}\right)}{4 \left(\tanh\left(\frac{\omega\beta}{2}\right) + 1 \right)^3 \left(\tanh^2\left(\frac{\omega\beta}{2}\right) + 1 \right)}, \end{aligned}$$

which in this case have the following explicit correlation

$$p_1 p_4 = p_2 p_3, \quad \text{with} \quad p_1 + p_2 + p_3 + p_4 = 1. \quad (50)$$

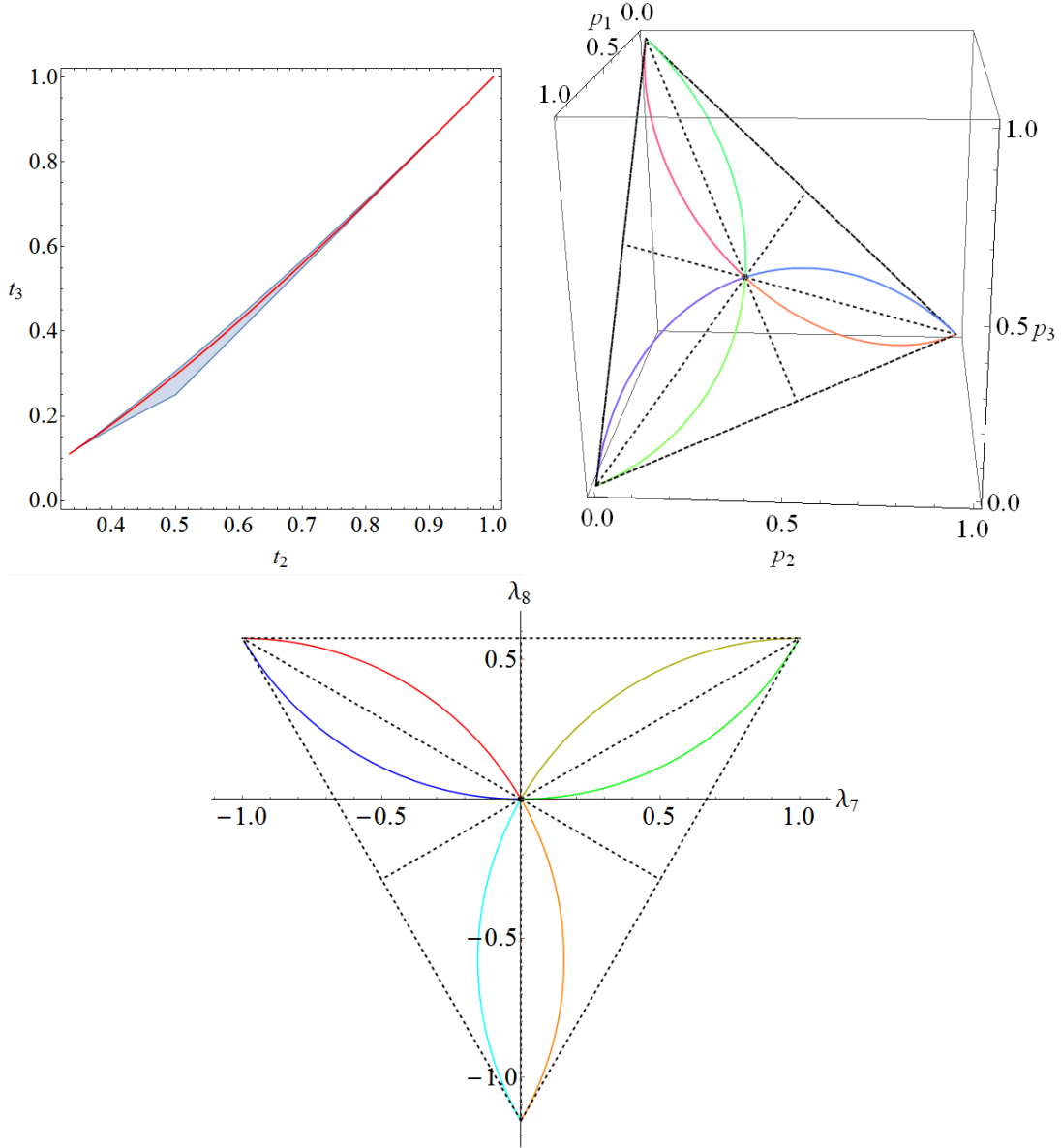


Figure 8. Left: curve defined by the thermal states of a qutrit crossing the allowed physical region which defines a valid quantum system, from the most mixed state ($t_2 = 1/3$, $t_3 = 1/9$) ($T \rightarrow \infty$) to the pure state state ($t_2 = t_3 = 1$) ($T \rightarrow 0$). Right: the same curve defined by the thermal states as seen in p -space follows a three-petal-flower-like structure. Bottom: The same flower-like structure is seen in λ -space.

By taking all the possible permutations of the probabilities we obtain 24 different curves, abbreviated in the following expression

$$p_j p_k = p_l p_m, \quad \text{with} \quad (j, k, l, m) = \pi(1, 2, 3, 4), \quad \pi \in \mathcal{S}_4. \quad (51)$$

The probabilities of Eq. (50) lead us to the Gell-Mann parameters (λ_{13} , λ_{14} , λ_{15}) which take the form

$$\lambda_{13} = \frac{1}{2} \tanh\left(\frac{\omega\beta}{2}\right) (\tanh(\omega\beta) + 1), \quad \lambda_{14} = \frac{\left(\tanh\left(\frac{\omega\beta}{2}\right) + 1\right) (3 \tanh(\omega\beta) + \text{sech}(\omega\beta) - 1)}{4\sqrt{3}},$$

$$\lambda_{15} = \frac{\tanh\left(\frac{\omega\beta}{2}\right) + \tanh(\omega\beta) + \text{sech}(\omega\beta) - 1}{\sqrt{6}}. \quad (52)$$

There are 24 different permutations for the labeling of the states, which define 24 different curves

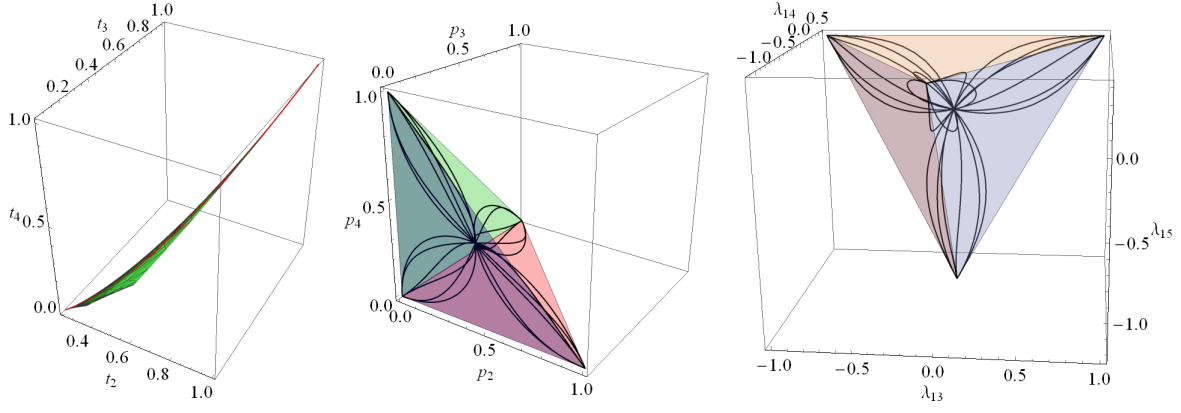


Figure 9. Left: curve defined by the thermal equilibrium states of a ququart crossing the allowed physical region which defines a valid quantum system, from the most mixed state ($t_2 = 1/4$, $t_3 = 1/16$, $t_4 = 1/64$) ($T \rightarrow \infty$) to the pure state state ($t_2 = t_3 = t_4 = 1$) ($T \rightarrow 0$). Center: the same curve defined by the thermal states as seen in p -space follows a three-petal-flower-like structure; all permutations of the labeling of the states have been taken. Right: The same flower-like structure is seen in λ -space. See text for details.

in λ -space. One of these satisfies

$$-2\lambda_{13} (4\sqrt{3}\lambda_{14} + 5\sqrt{6}\lambda_{15} - 6) + 8\lambda_{14}^2 + 2\lambda_{14} (2\sqrt{3} - 5\sqrt{2}\lambda_{15}) - 7\lambda_{15} (2\lambda_{15} + \sqrt{6}) = 0. \quad (53)$$

which gives us a path in λ -space. All such paths can be seen in Figure 9 (each petal consists of 6 of them).

4.3. Lipkin-Meshkov-Glick model

The Lipkin-Meshkov-Glick (LMG) model is a many body quantum system used in several fields like nuclear physics [41–43], condensed matter [44–46] and quantum optics [47], which can be written in terms of collective operators in the angular momentum algebra. The Hamiltonian of this model reads as

$$\mathbf{H} = 2\omega \mathbf{J}_z + \gamma_x \mathbf{J}_x^2 + \gamma_y \mathbf{J}_y^2. \quad (54)$$

The basis states can be written as follows

$$|N, n\rangle = \sqrt{\frac{(N-n)!}{N!n!}} \mathbf{J}_+^n |N, 0\rangle, \quad (55)$$

where $N = 2J$ denotes the number of particles, with $J \geq 1$; we have the quantum number $n = J + m$ and $\mathbf{J}_- |N, 0\rangle = 0$. The Hamiltonian has a symmetry under rotations by π radians along the Y axis. Thus the eigenstates have definite parity, and can be written as linear combinations of the form,

$$|s, e\rangle = \sum_{k=0}^{\lfloor N/2 \rfloor} C_{k,e}^s |N, 2k\rangle, \quad |s', o\rangle = \sum_{k=0}^{\lfloor (N-1)/2 \rfloor} D_{k,o}^{s'} |N, 2k+1\rangle, \quad (56)$$

where the integers s and s' take the values $s = 1, 2, \dots, \lceil \frac{N+1}{2} \rceil$ and $s' = 1, 2, \dots, \lfloor \frac{N+1}{2} \rfloor$, respectively. By means of the spin coherent states and the catastrophe theory it is possible to determine the quantum phase diagram for the ground state of the LMG model, in the limit $N \rightarrow \infty$. This diagram is determined by the locus of points in the control parameter space

$$(\gamma_x, \gamma_y) = (0, 0) \quad \text{if} \quad \gamma_x > -1, \quad \gamma_y > -1,$$

$$\begin{aligned}
\gamma_x &= -1, & \text{if } \gamma_y &\leq -1, \quad \gamma_y < \gamma_x, \\
\gamma_y &= -1, & \text{if } \gamma_x &\leq -1, \quad \gamma_y > \gamma_x, \\
\gamma_y &= \gamma_x, & \text{if } \gamma_x &\leq -1.
\end{aligned} \tag{57}$$

Notice that the intersection of even and odd energy surfaces yields a Maxwell set $\gamma_y = 1/\gamma_x$; in the region between the branches of this hyperbola there is no degeneracy between the energy levels of the LMG model, whereas in the exterior part degeneracy is present. By means of the Ehrenfest classification the order of the quantum phase transitions may be determined. One finds second order transitions when the straight lines $\gamma_x = -1$, $\gamma_y = -1$ and $\gamma_y = \gamma_x$ are crossed. When the line $\gamma_y = \gamma_x$ is traversed, first order transitions are exhibited. Finally if the point $(\gamma_x, \gamma_y) = (-1, -1)$ is crossed along the straight line $\gamma_y = -\gamma_x - 2$ a third order transitions is present [48].

Here, we will consider the LMG model for $N = 2$ particles ($J = 1$), given in units of 2ω as

$$\mathbf{H} = \mathbf{J}_z + g_x \mathbf{J}_x^2 + g_y \mathbf{J}_y^2,$$

where $g_x = \gamma_x/(2\omega)$ and $g_y = \gamma_y/(2\omega)$. Then thermal states associated to the Hamiltonian for $N = 2$ particles are given by the following density matrix,

$$\begin{aligned}
\rho &= \begin{pmatrix} \rho_o & 0 \\ 0 & \rho_e \end{pmatrix}, \quad \rho_o = \left(\frac{1}{2e^{\frac{\beta g_+}{2}} \cosh\left(\frac{1}{2}\beta\sqrt{g_-^2+4}\right) + 1} \right), \\
\rho_e &= \begin{pmatrix} \frac{e^{\frac{\beta g_+}{2}} \left(\cosh\left(\frac{1}{2}\beta\sqrt{g_-^2+4}\right) - \frac{2 \sinh\left(\frac{1}{2}\beta\sqrt{g_-^2+4}\right)}{\sqrt{g_-^2+4}} \right)}{2e^{\frac{\beta g_+}{2}} \cosh\left(\frac{1}{2}\beta\sqrt{g_-^2+4}\right) + 1} & -\frac{g_- e^{\frac{\beta g_+}{2}} \sinh\left(\frac{1}{2}\beta\sqrt{g_-^2+4}\right)}{\sqrt{g_-^2+4} \left(2e^{\frac{\beta g_+}{2}} \cosh\left(\frac{1}{2}\beta\sqrt{g_-^2+4}\right) + 1 \right)} \\ -\frac{g_- e^{\frac{\beta g_+}{2}} \sinh\left(\frac{1}{2}\beta\sqrt{g_-^2+4}\right)}{\sqrt{g_-^2+4} \left(2e^{\frac{\beta g_+}{2}} \cosh\left(\frac{1}{2}\beta\sqrt{g_-^2+4}\right) + 1 \right)} & \frac{e^{\frac{\beta g_+}{2}} \left(\frac{2 \sinh\left(\frac{1}{2}\beta\sqrt{g_-^2+4}\right)}{\sqrt{g_-^2+4}} + \cosh\left(\frac{1}{2}\beta\sqrt{g_-^2+4}\right) \right)}{2e^{\frac{\beta g_+}{2}} \cosh\left(\frac{1}{2}\beta\sqrt{g_-^2+4}\right) + 1} \end{pmatrix}, \tag{58}
\end{aligned}$$

where ρ_o is a 1×1 matrix and ρ_e is a 2×2 matrix, exhibiting the symmetry invariance of the Hamiltonian, since the Hilbert space divides itself into odd and even subspaces as mentioned previously. The eigenvalue of ρ_o

$$\rho_{11} = \frac{1}{1 + 2e^{\frac{\beta g_+}{2}} \cosh\left(\frac{1}{2}\beta\sqrt{g_-^2+4}\right)},$$

is the probability of finding the system in the odd state. For the even subspace ρ_e the eigenvalues

$$\rho_{22} = \frac{e^{\frac{1}{2}\beta(g_+ + \sqrt{g_-^2+4})}}{1 + 2e^{\frac{\beta g_+}{2}} \cosh\left(\frac{1}{2}\beta\sqrt{g_-^2+4}\right)}, \quad \rho_{33} = \frac{e^{\frac{1}{2}\beta(g_+ - \sqrt{g_-^2+4})}}{1 + 2e^{\frac{\beta g_+}{2}} \cosh\left(\frac{1}{2}\beta\sqrt{g_-^2+4}\right)},$$

stand for the probabilities of the ground and excited states of the system. We have defined $g_{\pm} := g_x \pm g_y$. We are here considering an ensemble of two-particles, with definite angular momentum $J = 1$, but without a well defined projection along the Z axes.

As the numeration of the eigenvalues of ρ is arbitrary, the probabilities can be represented by any permutation $(p_1, p_2, p_3) = \boldsymbol{\pi}(\rho_{11}, \rho_{22}, \rho_{33})$. The correlation between them depends exponentially on the temperature and Hamiltonian parameters $\beta(g_x + g_y)$ as

$$p_1^2 = e^{\beta(g_x + g_y)} p_2 p_3. \tag{59}$$

The invariants of the density matrix are found to be

$$t_2 = \frac{1 + 2e^{\beta g_+} \cosh\left(\beta\sqrt{g_-^2 + 4}\right)}{\left(1 + 2e^{\frac{\beta g_+}{2}} \cosh\left(\frac{1}{2}\beta\sqrt{g_-^2 + 4}\right)\right)^2}, \quad t_3 = \frac{1 + 2e^{\frac{3\beta g_+}{2}} \cosh\left(\frac{3}{2}\beta\sqrt{g_-^2 + 4}\right)}{\left(1 + 2e^{\frac{\beta g_+}{2}} \cosh\left(\frac{1}{2}\beta\sqrt{g_-^2 + 4}\right)\right)^3}. \quad (60)$$

Thus the thermal states can be located anywhere in the 2-simplex defined by the points (p_1, p_2, p_3) . For example when $\beta \rightarrow 0$ one gets the most mixed state, while for $\beta \rightarrow \infty$ the eigenvalues are equal to $(p_1 = 0, p_2 = 1, p_3 = 0)$; and due to the symmetry under the permutation group, all the regions can be reached by a thermal state of the LMG model. Given this, one can study the dependency of the eigenvalues (p_1, p_2, p_3) , the invariants t_2 and t_3 , and the Gell-Mann parameters λ_7 and λ_8 in terms of the temperature and the Hamiltonian parameters.

As one can see in the previous expressions, the system can be defined by the parameters $x = \beta g_+$ and $y = \beta\sqrt{g_-^2 + 4}$, which are used to visualize the different properties in a three-dimensional space. Since the energies of the LMG Hamiltonian can be written as $E_0 = g_+$, $E_{\pm} = \frac{1}{2}(g_+ \pm \sqrt{g_-^2 + 4})$, we may identify the parameters as $x = \beta E_0$ and $y = \beta(E_+ - E_-)$.

In Figure 10 the parametric plots for probabilities p_1 , p_2 , and p_3 for different values of the LMG Hamiltonian parameters g_x and g_y and for the case of angular momentum equal to one are shown. Each figure is plotted for a fixed temperature and each color corresponds to a different permutation of the three levels of the system. We emphasize that the points of each permutation are located within specific zones of the simplex, and each zone is delimited by a median, a bisector and the outer simplex boundary. The non-crossing of these zones indicates that the values of the probabilities maintain a certain order (for example, $p_1 > p_2 > p_3$) and there is no zone where this order is different. This is because the median and bisector lines are the points where two probabilities are equal and the allowed zones do not touch them due to the small value of the non-linearity of the system (in this case $g_x, g_y \in (-1, 1)$). Nonetheless, when the values of g_x and g_y grow larger (and so do the non-linearity) one can have two equal probabilities or any other possibility as one can see in Figure 11, where different crossings between the zones are shown. Specifically, this change of behavior (non-crossing versus crossing) has as a limit the situation where two probabilities are equal, and this takes place when $g_x = 1/g_y$. Also, in Figures 10 and 11, one can see that for a small temperature ($\beta \gg 1$) the system approaches a pure state (the ground state of the Hamiltonian), while for a large temperature ($\beta \ll 1$) the system approaches the most mixed state where $p_1 = p_2 = p_3 = 1/3$.

4.4. Ququart

For the angular momentum $j = 3/2$ the thermal density matrix for the LMG Hamiltonian model can be written as

$$\rho = \begin{pmatrix} \rho_o & 0 \\ 0 & \rho_e \end{pmatrix}, \quad (61)$$

with

$$\rho_o = \begin{pmatrix} \frac{e^{\beta} \left(x_1 \cosh\left(\frac{\beta x_1}{2}\right) - (g_+ + 2) \sinh\left(\frac{\beta x_1}{2}\right) \right)}{2x_1 \left(e^{\beta} \cosh\left(\frac{\beta x_1}{2}\right) + \cosh\left(\frac{\beta x_2}{2}\right) \right)} & -\frac{\sqrt{3}e^{\beta} g_- \sinh\left(\frac{\beta x_1}{2}\right)}{2e^{\beta} x_1 \cosh\left(\frac{\beta x_1}{2}\right) + 2x_1 \cosh\left(\frac{\beta x_2}{2}\right)} \\ -\frac{\sqrt{3}e^{\beta} g_- \sinh\left(\frac{\beta x_1}{2}\right)}{2e^{\beta} x_1 \cosh\left(\frac{\beta x_1}{2}\right) + 2x_1 \cosh\left(\frac{\beta x_2}{2}\right)} & \frac{e^{\beta} \left((g_+ + 2) \tanh\left(\frac{\beta x_1}{2}\right) + x_1 \right)}{2x_1 \left(e^{\beta} + \operatorname{sech}\left(\frac{\beta x_1}{2}\right) \cosh\left(\frac{\beta x_2}{2}\right) \right)} \end{pmatrix},$$

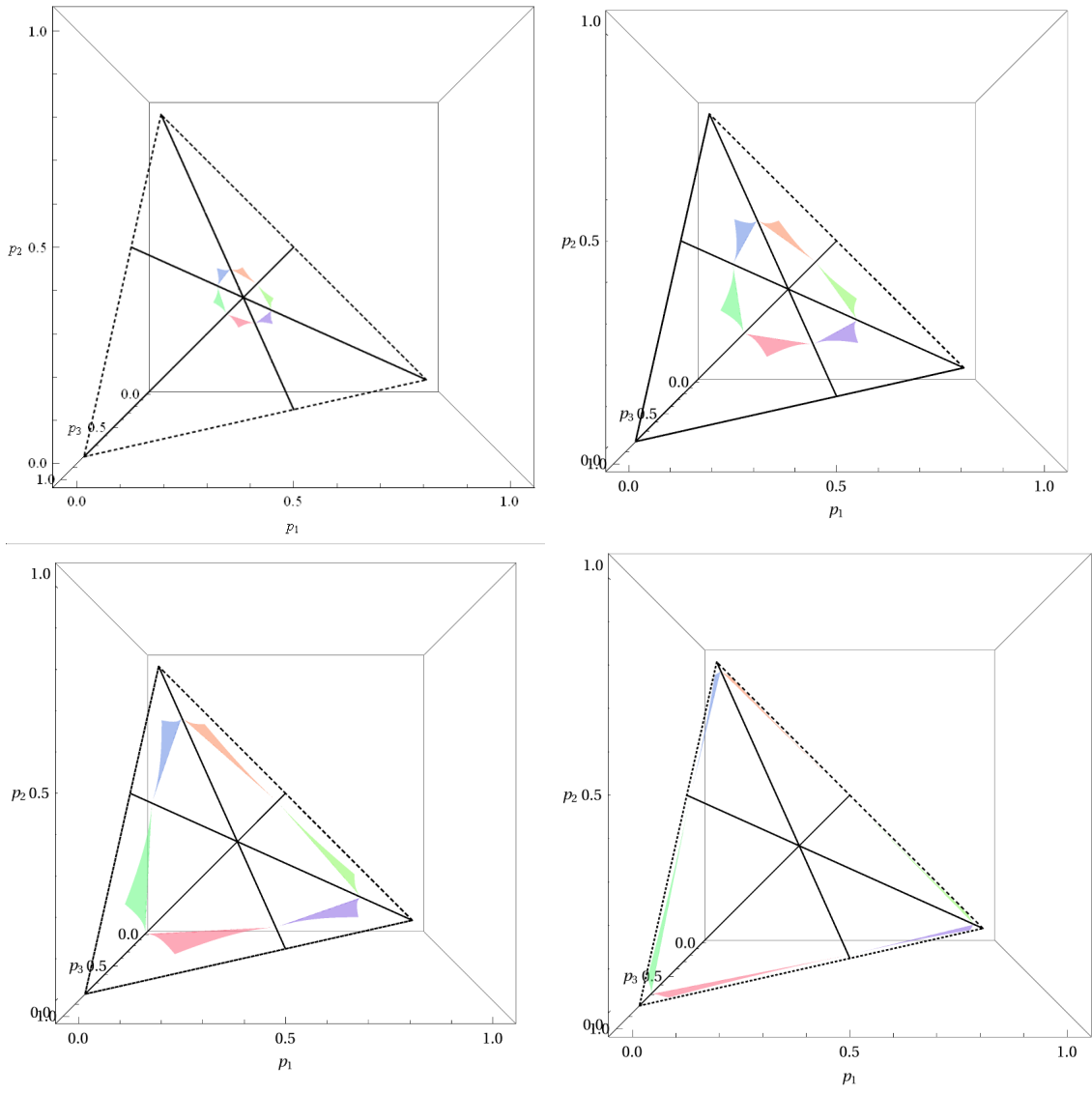


Figure 10. Probabilities for the three-level diagonal thermal equilibrium state defined by the LMG Hamiltonian model for a) $\beta = 1/5$, b) $\beta = 1/2$, c) $\beta = 1$, and d) $\beta = 2$. In all the cases $j = 1$ (qutrit) and $g_x, g_y \in (-1, 1)$.

$$\rho_e = \begin{pmatrix} \frac{(g_+ - 2) \sinh(\frac{\beta x_2}{2}) + x_2 \cosh(\frac{\beta x_2}{2})}{2x_2(e^\beta \cosh(\frac{\beta x_1}{2}) + \cosh(\frac{\beta x_2}{2}))} & -\frac{\sqrt{3}g_- \sinh(\frac{\beta x_2}{2})}{2e^\beta x_2 \cosh(\frac{\beta x_1}{2}) + 2x_2 \cosh(\frac{\beta x_2}{2})} \\ -\frac{\sqrt{3}g_- \sinh(\frac{\beta x_2}{2})}{2e^\beta x_2 \cosh(\frac{\beta x_1}{2}) + 2x_2 \cosh(\frac{\beta x_2}{2})} & \frac{x_2 \cosh(\frac{\beta x_2}{2}) - (g_+ - 2) \sinh(\frac{\beta x_2}{2})}{2x_2(e^\beta \cosh(\frac{\beta x_1}{2}) + \cosh(\frac{\beta x_2}{2}))} \end{pmatrix},$$

where $x_1 = \sqrt{(g_+ + 2)^2 + 3g_-^2}$ and $x_2 = \sqrt{(g_+ - 2)^2 + 3g_-^2}$.

The eigenvalues of the system are

$$\begin{aligned} p_1 &= \frac{e^{\frac{\beta x_2}{2}}}{2(e^\beta \cosh(\frac{\beta x_1}{2}) + \cosh(\frac{\beta x_2}{2}))}, & p_2 &= \frac{e^{-\frac{\beta x_2}{2}}}{2(e^\beta \cosh(\frac{\beta x_1}{2}) + \cosh(\frac{\beta x_2}{2}))}, \\ p_3 &= \frac{e^{\frac{\beta}{2}(x_1+2)}}{2(e^\beta \cosh(\frac{\beta x_1}{2}) + \cosh(\frac{\beta x_2}{2}))}, & p_4 &= \frac{e^{-\frac{\beta}{2}(x_1-2)}}{2(e^\beta \cosh(\frac{\beta x_1}{2}) + \cosh(\frac{\beta x_2}{2}))}. \end{aligned} \quad (62)$$

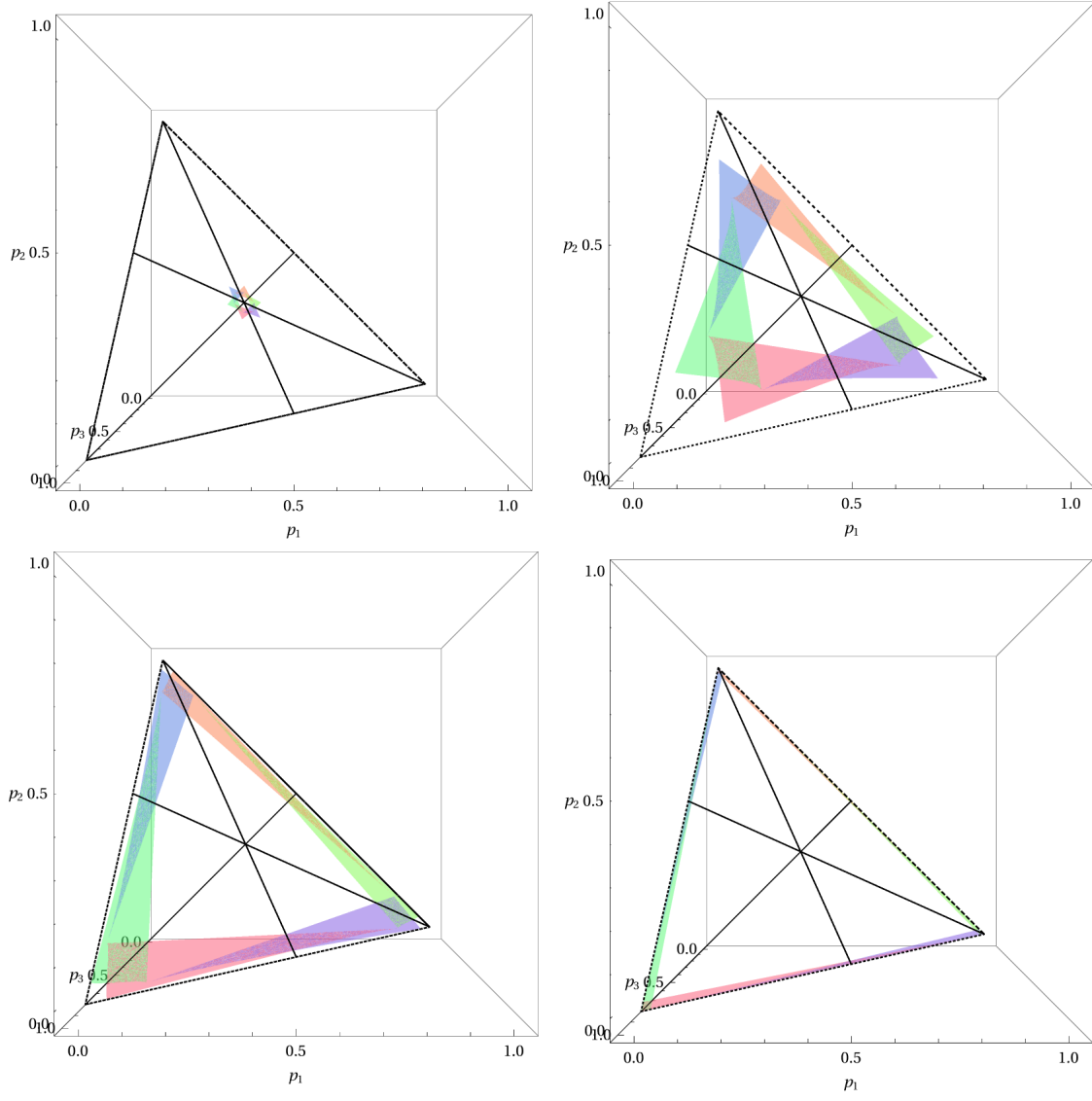


Figure 11. Probabilities for the three-level diagonal thermal equilibrium state defined by the LMG Hamiltonian for a) $\beta = 1/20$, b) $\beta = 1/2$, c) $\beta = 1$, and d) $\beta = 2$. In all the cases $j = 1$ (qutrit) and $g_x, g_y \in [-3, 3]$.

In this case we have a temperature dependent correlation function as the probabilities satisfy

$$p_1 p_2 = e^\beta p_3 p_4 . \quad (63)$$

The invariants t_2 , t_3 , and t_4 can be written as

$$t_2 = \frac{e^{2\beta} \cosh(\beta x_1) + \cosh(\beta x_2)}{2 \left(e^\beta \cosh\left(\frac{\beta x_1}{2}\right) + \cosh\left(\frac{\beta x_2}{2}\right) \right)^2}, \quad t_3 = \frac{e^{-\frac{3}{2}\beta(x_1-2)} + e^{\frac{3}{2}\beta(x_1+2)} + e^{-\frac{3}{2}\beta x_2} + e^{\frac{3}{2}\beta x_2}}{8 \left(e^\beta \cosh\left(\frac{\beta x_1}{2}\right) + \cosh\left(\frac{\beta x_2}{2}\right) \right)^3},$$

$$t_4 = \frac{e^{-2\beta(x_1-2)} + e^{2\beta(x_1+2)} + e^{-2\beta x_2} + e^{2\beta x_2}}{16 \left(e^\beta \cosh\left(\frac{\beta x_1}{2}\right) + \cosh\left(\frac{\beta x_2}{2}\right) \right)^4}, \quad (64)$$

while the Gell-Mann parameters λ_{13} , λ_{14} , and λ_{15} take the form

$$\lambda_{13} = \frac{1}{e^\beta \cosh\left(\frac{\beta x_1}{2}\right) \operatorname{csch}\left(\frac{\beta x_2}{2}\right) + \coth\left(\frac{\beta x_2}{2}\right)}, \quad \lambda_{14} = \frac{\cosh\left(\frac{\beta x_2}{2}\right) - e^{\beta + \frac{\beta x_1}{2}}}{\sqrt{3} \left(e^\beta \cosh\left(\frac{\beta x_1}{2}\right) + \cosh\left(\frac{\beta x_2}{2}\right) \right)},$$

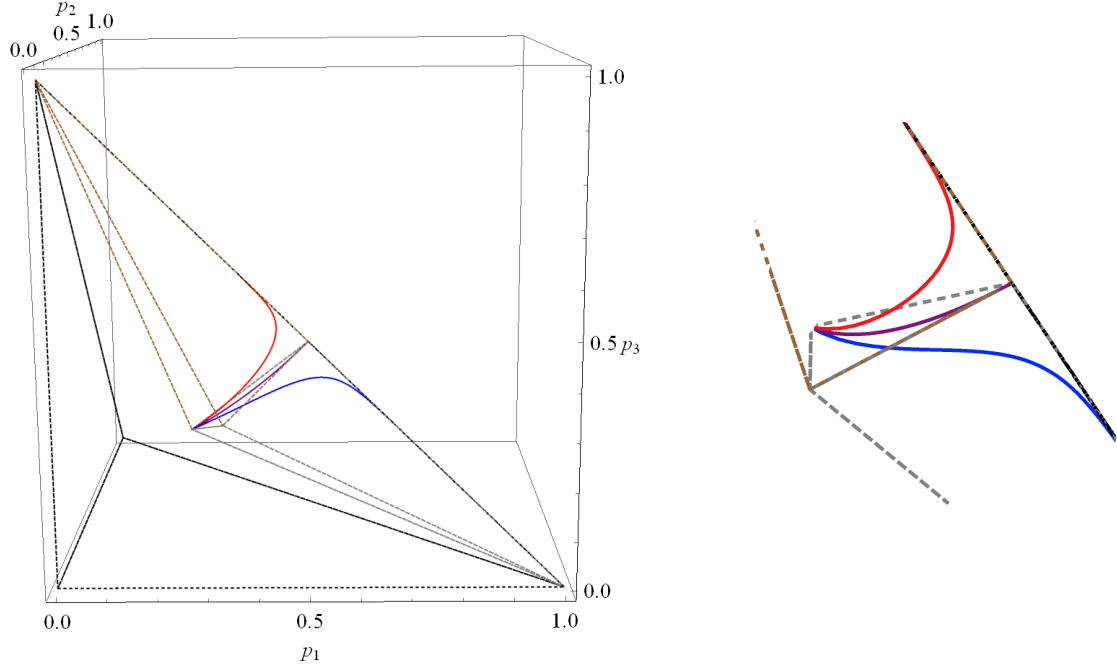


Figure 12. Left: Parametric plot for the probabilities p_1 , p_2 , and p_3 for the four-level thermal equilibrium state in the LMG Hamiltonian model, for $g_x = 1/4$, $g_y = 1$ (purple line); $g_x = 3/20$, $g_y = 1$ (blue line); $g_x = 7/20$, $g_y = 1$ (red line). Right: Zoom in around the centroid. See text for details.

$$\lambda_{15} = -\frac{1}{\sqrt{6}} \left(\frac{4e^\beta}{e^\beta + e^{\beta+\beta x_1} + 2e^{\frac{\beta x_1}{2}} \cosh\left(\frac{\beta x_2}{2}\right)} \right). \quad (65)$$

In the four-level system we have a similar behavior as in the qutrit case. Here the zones where the probabilities follow a certain order (say $p_1 > p_2 > p_3 > p_4$) are delimited by one of 24 different tetrahedrons inside the 3-simplex of Figure 5. Any crossing between these 24 tetrahedrons means that the intended order is no longer satisfied (for example $p_1 > p_2 > p_3 > p_4$ changes to $p_2 > p_1 > p_3 > p_4$ in two different tetrahedrons).

In the case of the LMG model the different behavior (non-crossing versus crossing of different zones) is given when the values of two probabilities are equal, and this takes place when $g_x = 1/(4g_y)$. Figure 12 shows the parametric plot for three different cases: $g_x = 1/(4g_y)$ (purple line) where the thermal evolution is given along the limit between two regions, $g_x < 1/(4g_y)$ (blue line) where the thermal evolution takes place inside one defined region, and $g_x > 1/(4g_y)$ (red line) where the thermal evolution takes place inside another region.

Similarly to the three-level system, in Figure 13 the parametric plot for the probabilities p_1 , p_2 , and p_3 are plotted for different temperature parameters β . As $T \rightarrow \infty$ we get the most mixed state, at the centroid, while for $T \rightarrow 0$ the possible states approach the edges of the simplex. The 24 possible permutations are taken into account in this figure and in this case there exist crossings between the different regions even for values where the non-linear parameters are smaller than one. In other words, the probabilities can have equal values in this system and sometimes perform an inversion of population.

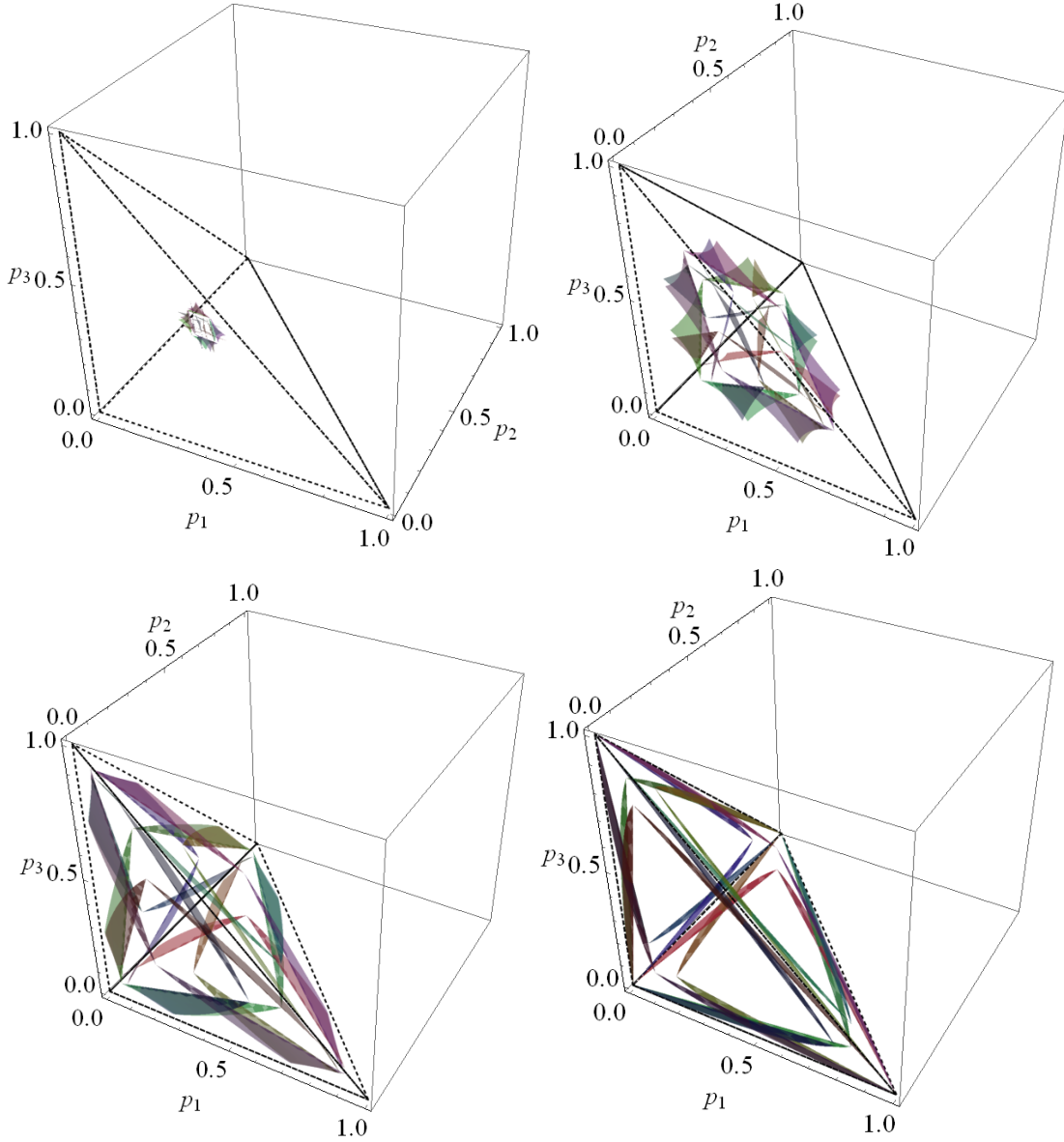


Figure 13. Probabilities for the four-level diagonal thermal equilibrium state defined by the LMG Hamiltonian for a) $\beta = 1/10$, b) $\beta = 1/2$, c) $\beta = 1$, and d) $\beta = 2$. In all the cases $j = 3/2$ (ququart) and $g_x, g_y \in [-1, 1]$.

5. Summary and concluding remarks

The PME yields the Boltzmann probability distribution function for any Hamiltonian system characterizing an ensemble of particles with fixed average energy, and one is able to maximize the von Neumann entropy and minimize the Helmholtz free energy. The diagonal representation of the density matrix is a very useful tool to exhibit the purity properties of quantum systems. In this work we have considered the probability (2- and 3-simplices), the Gell-Mann, and the invariant spaces. In all of them, one is able to visualize the purity properties of qutrit and ququart systems: when there is maximum mixture, to identify the regions where the eigenvalues exhibit triple or double degeneracies, and also the loci of points where all the eigenvalues are different. In order to do that, it was necessary to establish linear and non-linear maps between the mentioned representations, which additionally allow us to determine general geometric properties of the qutrit and ququart systems such as the following:

(i) trajectories in the p -, λ -, and t - spaces, by changing the temperature associated to the density matrix, and in this form visualize immediately the corresponding purity properties of the considered state; (ii) trajectories associated to fixed values of the invariants t_2 , t_3 , and t_4 (see Figs. 3, 4, 6, 7). For the thermal states associated to the linear Hamiltonian in the angular momentum operators it was possible to establish: (i) For the qutrit, the curves $p_1^2 = p_2 p_3$ and its corresponding permutations giving rise to three-petal-flower-like structure in the 2-simplex, and also the corresponding mapping to the λ space; in the t -space a trajectory with fixed values of t_2 and t_3 was shown (see Fig. 8); the double degeneracy happens when the Hamiltonian interaction strengths g_{\pm} describe hyperbolae with axes equal to 2ω . (ii) For the ququart with $p_1 p_4 = p_2 p_3$ and its corresponding permutations, similar geometric structures were determined, but now inside the corresponding 3-simplex (the tetrahedron). The analysis of the LMG Hamiltonian model includes the qutrit $J = 1$ and the ququart $J = 3/2$. For the qutrit, there is information of the quantum phase diagram by taking $\beta = 10$ and changing the interaction strengths of the Hamiltonian. Additionally, one finds very different trajectories for the same temperatures $\beta = 1/20, 1/2, 1, 2$ when constraining the values of g_x, g_y in the interval $[-1, 1]$, in contrast to the paths when g_x, g_y lie in the interval $[-3, 3]$ (see Figs. 10, 11). For the ququart, the three-dimensional representation is established for different fixed values of g_{\pm} and different temperatures (see Fig. 12). For $\beta = 1/20, 1/2, 1, 2$ the trajectories in the p -space are exhibited for g_x, g_y in the interval $[-1, 1]$, and we see that they move to the boundary of the tetrahedron in a similar manner as for the qutrit case.

We studied different ways to visualize a three-level and four-level quantum system through its diagonal form and applied these methods in the study of thermal states defined by a Hamiltonian linear in the angular momentum operators and another non-linear Hamiltonian given by the LMG model. Explicitly, we reviewed some aspects of the representations of such systems by using 1) the state probabilities given by the eigenvalues of the density matrix, 2) the density matrix invariants $\{t_n = \text{Tr}(\rho^n), n = 2, 3, \dots\}$, and 3) the generalized Gell-Mann parametrization.

For the linear and LMG model Hamiltonians we analyzed the different regions of the probability simplex which correspond to different sorting of the probability values and explored the behavior of the crossing between these regions when one changes the Hamiltonian parameters and also the temperature of the system.

The results above provide a much clearer understanding of the geometry and purity properties of qudit Hamiltonian systems.

References

- [1] Bennett C and Shor P 1998 *IEEE Transactions on Information Theory* **44** 2724–2742
- [2] Nielsen M A and Chuang I L 2011 *Quantum Computation and Quantum Information* (Cambridge University Press)
- [3] Werner R F 2001 *Quantum Information Theory - an Invitation* (Berlin, Heidelberg: Springer Berlin Heidelberg) pp 14–57 ISBN 978-3-540-44678-1
- [4] Zoller P, Beth T, Binosi D, Blatt R, Briegel H, Bruss D, Calarco T, Cirac J I, Deutsch D, Eisert J, Ekert A, Fabre C, Gisin N, Grangiere P, Grassl M, Haroche S, Imamoglu A, Karlson A, Kempe J, Kouwenhoven L, Kröll S, Leuchs G, Lewenstein M, Loss D, Lütkenhaus N, Massar S, Mooij J E, Plenio M B, Polzik E, Popescu S, Rempe G, Sergienko A, Suter D, Twamley J, Wendin G, Werner R, Winter A, Wrachtrup J and Zeilinger A 2005 *Eur. Phys. J. D* **36** 203–228
- [5] Benenti G, Casati G and Strini G 2007 *Principles of Quantum Computation and Information* vol I, II (World Scientific)
- [6] Grandy W T J 1997 *American Journal of Physics* **65** 466–476 ISSN 0002-9505
- [7] Shannon C E 1948 *The Bell System Technical Journal* **27** 379–423

- [8] Jaynes E T 1957 *Phys. Rev.* **106**(4) 620–630
- [9] Jaynes E T 1957 *Phys. Rev.* **108**(2) 171–190
- [10] Louisell W 1990 *Quantum Statistical Properties of Radiation* Wiley Classics Library (Wiley) ISBN 9780471523659
- [11] Shore J and Johnson R 1980 *IEEE Transactions on Information Theory* **26** 26–37
- [12] Heims S P and Jaynes E T 1962 *Rev. Mod. Phys.* **34**(2) 143–165
- [13] Calixto M, Mayorgas A and Guerrero J 2021 *Quantum Information Processing* **20** ISSN 1573-1332
- [14] Guerrero J, Mayorgas A and Calixto M 2022 *Quantum Information Processing* **21** ISSN 1573-1332
- [15] Mayorgas A, Guerrero J and Calixto M 2023 *Phys. Rev. E* **108**(2) 024107
- [16] Fano U 1957 *Rev. Mod. Phys.* **29**(1) 74–93
- [17] Byrd M S and Khaneja N 2003 *Phys. Rev. A* **68**(6) 062322
- [18] Kimura G 2003 *Phys. Lett. A* **314** 339–349 ISSN 0375-9601
- [19] Akhtarshenas S J 2007 *Opt. Spectrosc.* **103** 411–415
- [20] Bertlmann R A and Krammer P 2008 *J. Phys. A: Mathematical and Theoretical* **41** 235303
- [21] Brüning E, Mäkelä H, Messina A and Petruccione F 2012 *J. Modern Optics* **59** 1–20
- [22] Procesi C 1978 *Advances in Mathematics* **29** 219–225 ISSN 0001-8708
- [23] Procesi C 2007 *Lie Groups: An approach through Invariants and representations* (Springer New York, NY)
- [24] Curtiss D R 1918 *Annals of Mathematics* **19** 251–278 ISSN 0003486X
- [25] Arvind, Mallesh K S and Mukunda N 1997 *J. Phys. A: Mathematical and General* **30** 2417
- [26] Khanna G, Mukhopadhyay S, Simon R and Mukunda N 1997 *Ann. of Phys.* **253** 55–82 ISSN 0003-4916
- [27] Kuś M and Życzkowski K 2001 *Phys. Rev. A* **63**(3) 032307
- [28] Bengtsson I and Życzkowski K 2006 *Geometry of quantum states: An introduction to quantum entanglement* (Cambridge University Press)
- [29] Tay B A and Zainuddin H 2008 *Chinese Physics Letters* **25** 1923
- [30] Gerdt V P, Khvedelidze A M and Palii Y G 2014 *J. of Math. Sciences* **200** 682–689
- [31] Grunbaum B 2009 *Configurations of Points and Lines* Graduate studies in mathematics (Providence, RI: American Mathematical Society)
- [32] Hirschfeld J W P 1986 *Finite projective spaces of three dimensions* Oxford Mathematical Monographs (London, England: Oxford University Press)
- [33] Rau A R P 2021 *Symmetry* **13** ISSN 2073-8994 URL <https://www.mdpi.com/2073-8994/13/9/1732>
- [34] Reichl L E 2016 *A Modern Course in Statistical Physics* 4th ed Physics textbook (Wiley) ISBN 978-3-527-41349-2
- [35] Linden N, Popescu S and Wootters W K 2002 *Phys. Rev. Lett.* **89**(20) 207901
- [36] Goldstein S, Lebowitz J L, Tumulka R and Zanghì N 2006 *Phys. Rev. Lett.* **96**(5) 050403
- [37] Tasaki H 1998 *Phys. Rev. Lett.* **80**(7) 1373–1376
- [38] Coxeter H S M 1948 *Regular Polytopes* (Methuen & Co. Ltd., London)
- [39] Gilmore R 2005 *Lie Groups, Lie Algebras, and Some of Their Applications* Dover Books on Mathematics (Dover Publications) ISBN 9780486131566
- [40] Brüning E, Mäkelä H, Messina A and Petruccione F 2012 *Journal of Modern Optics* **59** 1
- [41] Lipkin H J, Meshkov N and Glick A J 1965 *Nucl. Phys.* **62** 188
- [42] Meshkov N, Glick A J and Lipkin H J 1965 *Nucl. Phys.* **62** 199
- [43] Glick A J, Lipkin H J and Meshkov N 1965 *Nucl. Phys.* **62** 211
- [44] Botet R, Jullien R and Pfeuty P 1982 *Phys. Rev. Lett.* **49**(7) 478–481
- [45] Botet R and Jullien R 1983 *Phys. Rev. B* **28**(7) 3955–3967
- [46] Pérez-Campos C, González-Alonso J R, Castaños O and R L 2010 *Annals of Physics* **325** 325–344
- [47] Kitagawa M and Ueda M 1993 *Phys. Rev. A* **47**(6) 5138–5143
- [48] Castaños O, López-Peña R, Nahmad-Achar E and Hirsch J G 2012 *J. Phys.: Conf. Ser.* **403** 012003